Chemical Science

ROYAL SOCIETY OF CHEMISTRY

EDGE ARTICLE

View Article Online
View Journal | View Issue

Cite this: *Chem. Sci.*, 2024, **15**, 17128

All publication charges for this article have been paid for by the Royal Society of Chemistry

Received 18th July 2024
Accepted 23rd September 2024

DOI: 10.1039/d4sc04796f

rsc.li/chemical-science

Tether-entangled conjugated helices†

Ke Jin,[ab] Zuo Xiao,[*ab] Huidong Xie,[ab] Xingxing Shen,[*c] Jizheng Wang,[d] Xiangyu Chen,[e] Zhijie Wang,[f] Zujin Zhao,[g] Keyou Yan,[h] Yong Ding[i] and Liming Ding[*ab]

A new design concept, tether-entangled conjugated helices (TECHs), is introduced for helical polyaromatic molecules. TECHs consist of a linear polyaromatic ladder backbone and periodically entangling tethers with the same planar chirality. By limiting the length of tether, all tethers synchronously bend and twist the backbone with the same manner, and change it into a helical ribbon with a determinate helical chirality. The 3D helical features are customizable *via* modular synthesis by using two types of synthons, the planar chiral tethering unit (C_2 symmetry) and the docking unit (C_{2h} symmetry), and no post chiral resolution is needed. Moreover, TECHs possess persistent chiral properties due to the covalent locking of helical configuration by tethers. Concave-type and convex-type oligomeric TECHs are prepared as a proof-of-concept. Unconventional double-helix π-dimers are observed in the single crystals of concave-type TECHs. Theoretical studies indicate the smaller binding energies in double-helix π-dimers than conventional planar π-dimers. A concentration-depend emission is found for concave-type TECHs, probably due to the formation of double-helix π-dimers in the excited state. All TECHs show strong circularly polarized luminescence (CPL) with dissymmetric factors ($|g_{lum}|$) generally over 10^{-3}. Among them, the **(*P*)-T4-^{t}Bu** shows the highest $|g_{lum}|$ of 1.0×10^{-2} and a high CPL brightness of 316 M^{-1} cm^{-1}.

Introduction

Helical polyaromatic molecules have attracted significant interest in recent years due to their aesthetically pleasing molecular structures, unique chemical and physical properties, and diverse applications.[1–17] Helicenes and twistacenes are two archetypes that have been extensively investigated (Fig. 1a).[18,19] Helicenes are formed of consecutively ortho-fused aromatic or heteroaromatic rings.[20–24] The steric repulsion between the spatially adjacent rings or groups endows helicenes with a spiral-staircase-shaped backbone and a helical conjugated system. The helical axis is near orthogonal to the π-surface of aromatic rings. Various helicenes and helicenoids like carbohelicenes,[25–28] heterohelicenes,[29–39] metallahelicenes,[40–45] multiple helicenes,[46–54] and expanded helicenes[55–64] have been developed. Twistacenes are twisted acenes or benzannulated acenes with steric crowdedness around the periphery.[65–83] The crowdedness causes conformational distortion and induces the backbone to adopt a helical conformation, where the helical axis is near parallel to the π-surface of aromatic rings of acenes. Despite structural differences, helicenes and twistacenes share in common that their helical geometry is caused by minimizing the unfavored steric interactions in the planar conformation against the energy cost of distortion.[65,84] Thus, the steric effect plays a vital role in deciding the helical structure and configurational stability for helicenes and twistacenes. Just for this reason, challenges like the difficulty in synthesis and chiral resolution, dynamic variation of the helical structures, multiple coexisting conformers, and easily happening racemization (especially for the shorter ones) have accompanied helicenes and twistacenes.[47,48,63,85–96]

Herein, we report a new design of helical polyaromatic molecules, the tether-entangled conjugated helices (TECHs) (Fig. 1a). TECHs contain two parts of structural elements, the linear ladder-type polyaromatic backbone[97–103] and the periodically entangling tethers with the same planar chirality. All tethers stretch across the backbone and locate in one side of the molecular plane. By limiting the length of tether, all tethers can

[a]*Center for Excellence in Nanoscience (CAS), Key Laboratory of Nanosystem and Hierarchical Fabrication (CAS), National Center for Nanoscience and Technology, Beijing 100190, China. E-mail: xiaoz@nanoctr.cn; ding@nanoctr.cn*

[b]*University of Chinese Academy of Sciences, Beijing 100049, China*

[c]*College of Chemical Engineering, Hebei Normal University of Science and Technology, Qinhuangdao 066004, China. E-mail: sxx3694@hevttc.edu.cn*

[d]*Institute of Chemistry, Chinese Academy of Sciences, Beijing 100190, China*

[e]*Beijing Institute of Nanoenergy and Nanosystems, Chinese Academy of Sciences, Beijing 101400, China*

[f]*Institute of Semiconductors, Chinese Academy of Sciencess, Beijing 100083, China*

[g]*State Key Laboratory of Luminescent Materials and Devices, South China University of Technology, Guangzhou 510640, China*

[h]*School of Environment and Energy, South China University of Technology, Guangzhou 510006, China*

[i]*Beijing Key Laboratory of Novel Thin-Film Solar Cells, North China Electric Power University, Beijing 102206, China*

† Electronic supplementary information (ESI) available. CCDC 2354646 and 2354656–2354661. For ESI and crystallographic data in CIF or other electronic format see DOI: https://doi.org/10.1039/d4sc04796f

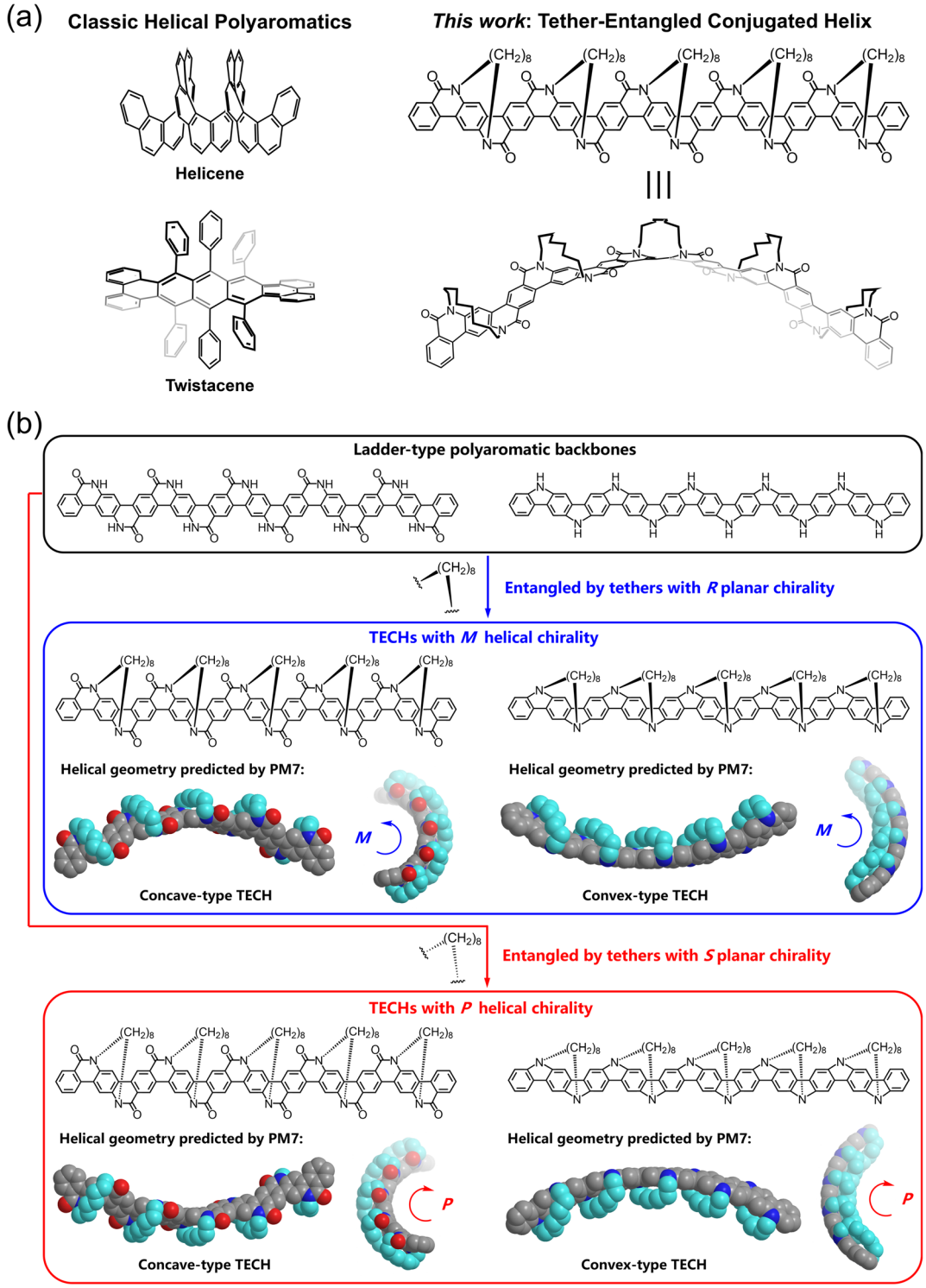

Fig. 1 (a) Classic helical polyaromatics, helicene and twistacene, and tether-entangled conjugated helix in this work. (b) The design concept of TECHs. Note: the geometries were optimized at PM7 level; hydrogens are omitted for clarity; the tethers are highlighted in sky blue.

synchronously introduce chiral strain to the backbone, and bend and twist the backbone with the same manner. As a result, the backbone is coiled up into a spiral aromatic ribbon with a determinate helical chirality. Different from helicenes and twistacenes, TECHs have following features: (1) the helical geometry of TECHs is no longer decided by the steric effect but by the chiral strain induced from the entangling tethers; (2) the helical chirality of TECHs is exclusive and only decided by the planar chirality of tether; (3) TECHs are static helices with constrained conformational variation; (4) because of the

covalent locking of the helical conformation by tethers, TECHs have high configurational stability and persistent chiral properties; (5) the helical structures and chirality of TECHs are customizable by modular synthesis, and no post chiral resolution is needed. In this paper, we introduce the design concept and synthesis analysis for TECHs. Two kinds of TECHs, the concave-type and convex-type oligomeric TECHs, were successfully prepared as a proof-of-concept. Moreover, the concave-type TECH molecules have shown interesting aggregation and chiroptical properties. These molecules can form double-helix dimers *via* an unconventional embracement-like π–π interaction and exhibit strong circularly polarized luminescence (CPL)[104–106] capability.

Results and discussion

Design concept and synthesis analysis

To better describe the design concept of TECHs, two typical ladder-type polyaromatic skeletons, the ladder aromatic lactams[107–113] and the ladder oligo(*p*-aniline)s,[114–119] are used as the backbones and the 8-carbons alkyl chains are used as the entangling tethers for building the models of TECHs (Fig. 1b). As shown in Fig. 1b, when using five *R*-planar-chirality (R_p) tethers to entangle the 21-fused-rings ladder aromatic lactams and the 21-fused-rings ladder oligo(*p*-aniline)s backbones, all tethers locate in front of the molecular plane, connecting two adjacent bridge nitrogen atoms from top left to bottom right. Due to the geometrical mismatch between backbones and tethers, strain is generated. All tethers synchronously curl the backbones into helical ribbons with the *M* chirality. The major difference for the two helical ribbons is the spatial location of the entangling tethers. In the case of helical ladder aromatic lactams, all tethers locate in the outer space of the helical structure, covering the convex surface and leaving the concave surface being exposed, whereas in the case of helical ladder oligo(*p*-aniline)s, all tethers locate in the inner space of the helical structure, covering the concave surface and leaving the convex surface being exposed. We define the former as the concave-type TECHs and the latter as the convex-type TECHs. The cause of this structural difference is due to the different bending direction of the backbones by the tethers. For concave-type TECHs, the bending is toward the opposite side of tethers, whereas for convex-type TECHs, the bending is toward the tethers' side. When using five *S*-planar-chirality (S_p) tethers to entangle the ladder aromatic lactams and ladder oligo(*p*-aniline)s, all tethers locate in back of the molecular plane. This time, both helical ribbons show the *P* chirality and mirror-imaged structures as compared to the *M*-helices. Therefore, the helical chirality of TECHs is only decided by the planar chirality of tether. The tether length has significant influence to the helical structures of TECHs. As shown in Fig. S1,† longer tethers like C10 or C12 alkyl chains induce little or neglectable chiral strain to the aromatic backbones, leading to less obvious or no helical characteristics. In sharp contrast, shorter tethers like C6 alkyl chains bring larger chiral strain and a higher degree of coiling to the backbones. From the above, it can be seen that the linear polyaromatic ladder backbone and the periodic homochiral entangling tethers in a limited length are the key factors for TECHs. Together they decide the helical shape of TECHs.

The synthesis analysis of TECHs is shown in Fig. 2. It is important to note that some helical ladder polymers and oligomers (conjugated or partially conjugated) have been synthesized by developing defect-free annulation reactions[120–123] and the use of axial,[124–126] planar[127,128] and helical[129–131] chiral building units. Inspired by these works and also the synthesis of ladder-type conjugated polymers and oligomers,[97,103,132–138] we considered that TECHs can be constructed *via* modular synthesis by using two types of synthons. The first one we call the chiral tethering unit, which has a planar chiral macrocyclic structure with the C_2 symmetry and four potential reactive sites (two a1 sites and two b1 sites). The second one we call the docking unit, which has the C_{2h} symmetry and four potential reactive sites (two a2 sites and two b2 sites). If a1 site can selectively bond with a2 site, b1 site can selectively bond with b2 site and no racemization happens for the chiral tethering unit during reaction, we can alternately dock the two building units and generate polymeric TECHs (Fig. 2b). To synthesize oligomeric TECHs, additional terminal units are required. The terminal units are similar to the docking unit but with only one side of reactive sites. Taking the oligomeric TECHs in Fig. 1b for examples, their synthesis can be achieved by using five chiral tethering units, four docking units and two terminal units (Fig. 2c). From the above, it can be concluded that three conditions are required for the synthesis of TECHs: (1) the prepared C_2-symmetric chiral tethering units and C_{2h}-symmetric docking units; (2) the selective bonding (a1 to a2, b1 to b2) between the chiral tethering unit and docking unit; (3) no racemization for the chiral tethering units during the reaction. If all the three conditions are satisfied, various TECHs with exclusive 3D geometrical characteristics (*e.g.* helical diameters and pitches) and chirality are customizable through the above modular synthesis. Fig. S2† shows some designed TECH molecules and their predicted helical structures by PM7.[139] It can be seen that even small structural modifications on the chiral tethering units or docking units can lead to dramatical change of the 3D helical geometries.

Synthesis of oligomeric TECHs

Guided by the design concept of TECHs, we start the preparation of oligomeric TECHs. First, we accomplished the synthesis of chiral tethering units **(S_p)-3** and **(R_p)-3** (Scheme 1). Treating 2,5-dibromoterephthalic acid with diphenylphosphoryl azide, triethylamine and the chiral auxiliary (*S*)-1-phenylethanol gave (*S*,*S*)-1 in 80% yield. Treating (*S*,*S*)-1 with 1,8-dibromooctane in diluted solution gave a pair of separable macrocyclic diastereomers (S,S_p,S)-2 and (S,R_p,S)-2 in 26% and 13% yield, respectively. The structures and the absolute configurations for (S,S_p,S)-2 and (S,R_p,S)-2 were unambiguously confirmed by single crystal X-ray diffraction (SCXRD). Treating (S,S_p,S)-2 or (S,R_p,S)-2 with trifluoroacetic acid completely removed the chiral auxiliaries and afforded the planar chiral compounds **(S_p)-3** or **(R_p)-3** in 94% or 95% yield, respectively. The

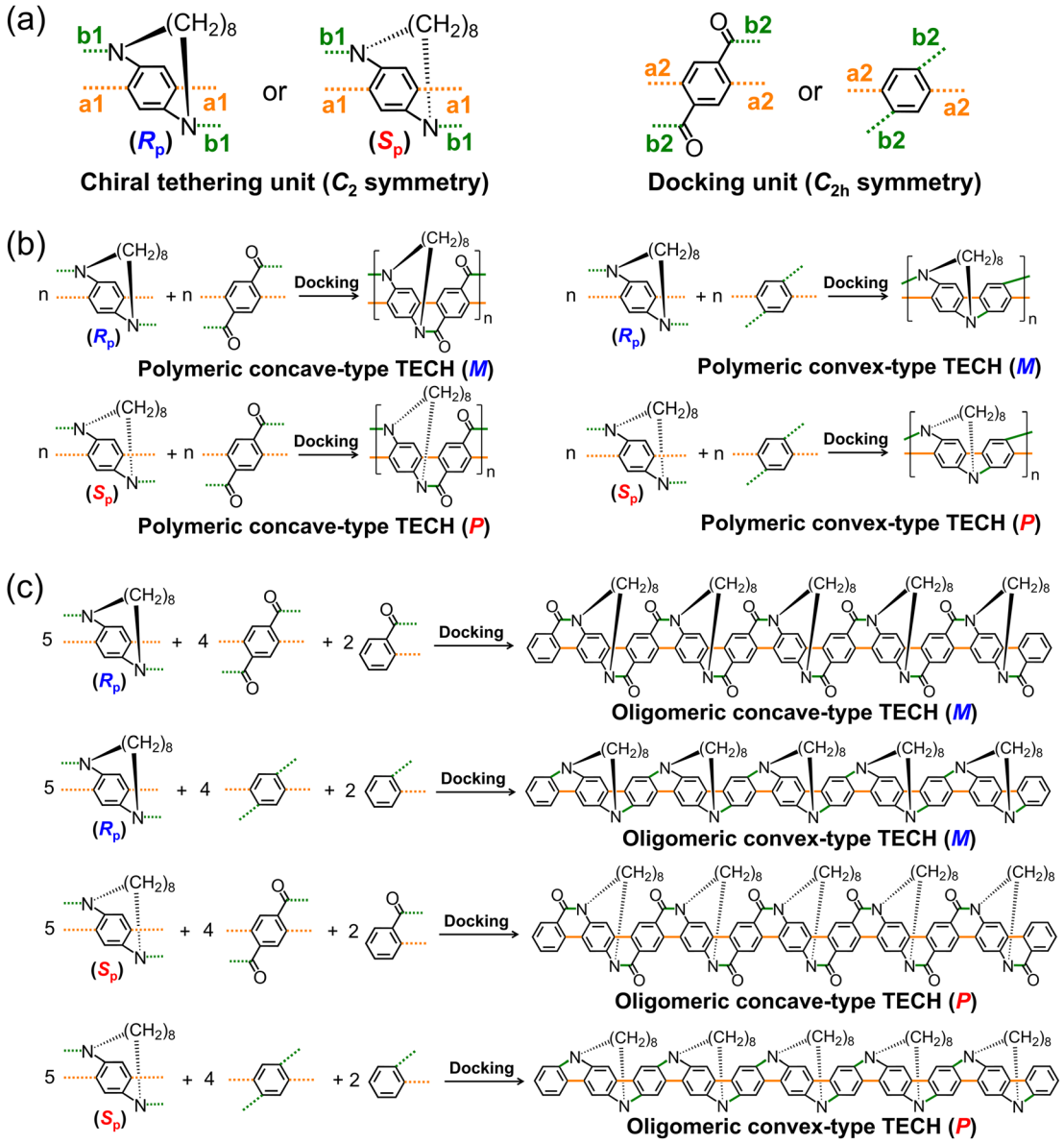

Fig. 2 The synthesis analysis of TECHs: (a) the chiral tethering unit and the docking unit; (b) modular synthesis of polymeric TECHs; (c) modular synthesis of oligomeric TECHs.

enantiomeric excess (ee) values for **(S_p)-3** and **(R_p)-3** are 98.4% and 99.7%, respectively. **(S_p)-3** and **(R_p)-3** are C_2-symmetric molecules with four potential reactive sites, two aryl bromides (a1 site) and two amines (b1 site), satisfying the requirements as chiral tethering units. Bearing in mind that the chiral tethering units should not undergo racemization during TECH synthesis, we tested the configurational stability of **(S_p)-3** and **(R_p)-3** by heating them at 130 °C for 48 hours. It was found that neither **(S_p)-3** nor **(R_p)-3** underwent racemization after the thermal treatment (Fig. S3†), suggesting the sufficiently high racemization barrier. This result indicates that **(S_p)-3** and **(R_p)-3** are suitable chiral tethering units for the synthesis of TECHs. We also tried to synthesis chiral tethering units with shorter tethers like C7 or C6 alkyl chains. However, no isolable product was obtained in the macrocyclization reaction. This could be due to the too high internal strain in these molecules, making them difficult to generate and stabilize.

Next, we started to synthesize the *P* and *M* oligomeric concave-type TECHs from **(S_p)-3** and **(R_p)-3**, respectively (Scheme 2). For synthesizing shorter TECHs like **(*P*)-T1**, **(*P*)-T1-^{t}Bu**, **(*P*)-T2-^{t}Bu** and **(*P*)-T3-^{t}Bu**, the basic strategy is constructing the amide oligomers first (accomplishing the b1 to b2 bonding) and then conducting the Pd-catalyzed consecutive intramolecular C–H arylations[140–145] (accomplishing the a1 to a2 bonding, *i.e.* linear ladderization) at one time to give the target molecules. The synthesis of **(*P*)-T3-^{t}Bu** is used as an example for a detailed description. Amidation of **(S_p)-3** with methyl 4-(chlorocarbonyl)benzoate afforded the bis-amide (S_p)-4-CO_2Me in 88% yield. Hydrolysis of (S_p)-4-CO_2Me with KOH gave (S_p)-4-CO_2H in 97% yield. Then, (S_p)-4-CO_2H was converted to acyl

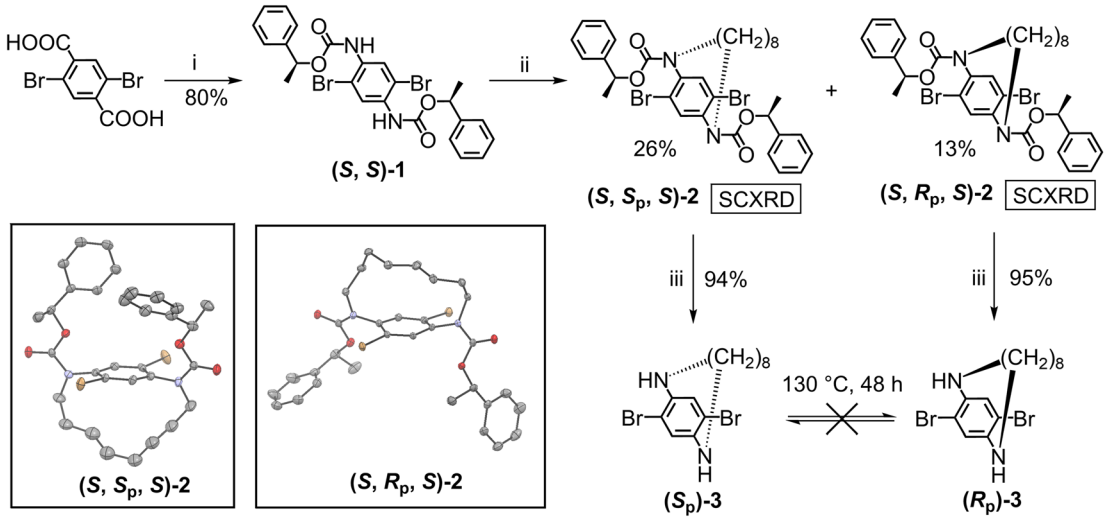

Scheme 1 Synthesis of the chiral tethering units (S_p)-3 and (R_p)-3. Reaction conditions: (i) $(PhO)_2P{=}ON_3$/Et_3N/(*S*)-1-phenylethanol, toluene, 80 °C; (ii) Cs_2CO_3/KI/1,8-dibromooctane, DMF, 80 °C; (iii) TFA, CH_2Cl_2, r.t.

chloride and reacted with 2 equiv. of **(S_p)-3** and afforded the tetrakis-amide (S_p,S_p,S_p)-7 in 95% yield. Amidation of (S_p,S_p,S_p)-7 with 4-*tert*-butylbenzoyl chloride afforded the hexakis-amide (S_p,S_p,S_p)-8-^{t}Bu in 96% yield. Finally, **(*P*)-T3-^{t}Bu** was obtained in 61% yield through the Pd-catalyzed linear ladderization (six new C–C bonds formed). It can be seen that the yields for the last ladderization step continuously drop from ~90% for **(*P*)-T1** and **(*P*)-T1-^{t}Bu** to 61% for **(*P*)-T3-^{t}Bu**. This is caused by two reasons. The first one is the accompanied debromination side reaction in the Pd-catalyzed C–H arylation.[146] When the number of bromine atoms in the substrate increases, the debromination become more severe. The second one is the generation of curved ladderization isomers. As shown in Fig. S4 and S5,† it is possible to generate two and three isomers in the last step of **(*P*)-T2-^{t}Bu** and **(*P*)-T3-^{t}Bu**, respectively. For both cases, the target linear ladderization isomers are always the most thermodynamically favored products, whereas the curved isomers are less favored due to the steric crowdness on backbone. The DFT-optimized structures indicate helicene-like segments in these curved isomers. Despite being energetically unfavorable, small amount of **(*P*)-T2-^{t}Bu** curved isomer (7% yield), and **(*P*)-T3-^{t}Bu** curved-1 isomer (15% yield) and curved-2 isomer (7% yield) were observed and isolated from the low-polarity side products of **(*P*)-T2-^{t}Bu** and **(*P*)-T3-^{t}Bu**, respectively (see ESI†). Characterization data confirmed the structures shown in Fig. S4 and S5.† This generation of curved isomers highlights the need for strict control of the symmetry of docking unit in TECH synthesis, that is, the docking unit must keep the C_{2h} symmetry to ensure that all tethers can be located on the same side of the molecular plane. In curved isomers, the symmetry of docking unit changed from C_{2h} to C_{2v}, thus leading to tethers on both sides of the molecular plane. This deviates the design target of TECHs.

Due to the increasing debromination side products and the curved ladderization isomers, the one-step ladderization strategy is not applicable for longer TECHs like **(*P*)-T4-^{t}Bu** and **(*P*)-T5-^{t}Bu**. Therefore, we adopted a stepwise ladderization strategy for the synthesis of **(*P*)-T4-^{t}Bu** and **(*P*)-T5-^{t}Bu**. For **(*P*)-T4-^{t}Bu**, we conducted the first-step ladderization to build the core structure (*P*)-T2-CO_2H. The synthesis is similar to **(*P*)-T2-^{t}Bu** (Scheme S1†). Starting from (*P*)-T2-CO_2H, the amide precursor (S_p,P,S_p)-10-^{t}Bu was prepared through two amidation processes. Finally, **(*P*)-T4-^{t}Bu** was obtained in 43% yield from (S_p,P,S_p)-10-^{t}Bu through the second-step ladderization. For **(*P*)-T5-^{t}Bu**, the first-step ladderization afforded the core structure (*P*)-T3-CO_2H. The synthesis is similar to **(*P*)-T3-^{t}Bu** (Scheme S2†). Then, the amide precursor (S_p,P,S_p)-12-^{t}Bu was prepared, and **(*P*)-T5-^{t}Bu** was obtained in 23% yield from (S_p,P,S_p)-12-^{t}Bu through the second-step ladderization. For all *M* concave-type oligomers (**(*M*)-T1-^{t}Bu**, **(*M*)-T2-^{t}Bu**, **(*M*)-T3-^{t}Bu**, **(*M*)-T4-^{t}Bu**, **(*M*)-T5-^{t}Bu**), their syntheses are identical to their *P*-counterparts but using **(R_p)-3** as the starting material (Scheme 2b). The detailed synthetic routes are given in the Scheme S3.†

Next, we synthesized the convex-type TECHs, **(*P*)-T1-convex**, **(*P*)-T2-convex**, **(*M*)-T1-convex**, and **(*M*)-T2-convex** (Scheme 3). First, 1 equiv. of **(S_p)-3** coupled with 2 equiv of 2-(2,5-difluorophenyl)-4,4,5,5-tetramethyl-1,3,2-dioxaborolane *via* the Suzuki reaction and gave (S_p)-13 in 85% yield. Then, ^{t}BuOK-promoted intramolecular nucleophilic ring-closure reaction[119] transformed (S_p)-13 to **(*P*)-T1-convex** in 84% yield. For **(*P*)-T2-convex**, 1 equiv. of **(S_p)-3** first coupled with 1 equiv. of 2-(2,5-difluorophenyl)-4,4,5,5-tetramethyl-1,3,2-dioxaborolane to give (S_p)-14 in 55% yield. (S_p)-14 then coupled with 2,5-difluorobenzene-1,4-diboronicacidbis(pinacol)ester and gave (S_p)-15 in 52% yield. Finally, ^{t}BuOK-promoted ring-closure reaction gave **(*P*)-T2-convex** in 17% yield. Considering the quite low yield of the final step of **(*P*)-T2-convex**, we didn't try to synthesis longer oligomeric convex-type TECHs. For **(*M*)-T1-convex** and **(*M*)-T2-convex**, they were synthesized similarly as their *P*-counterparts but with **(R_p)-3** as the starting material.

All TECH molecules as well as their intermediates were characterized by nuclear magnetic resonance (NMR) and high-resolution mass (HRMS) spectroscopic methods (see ESI†).

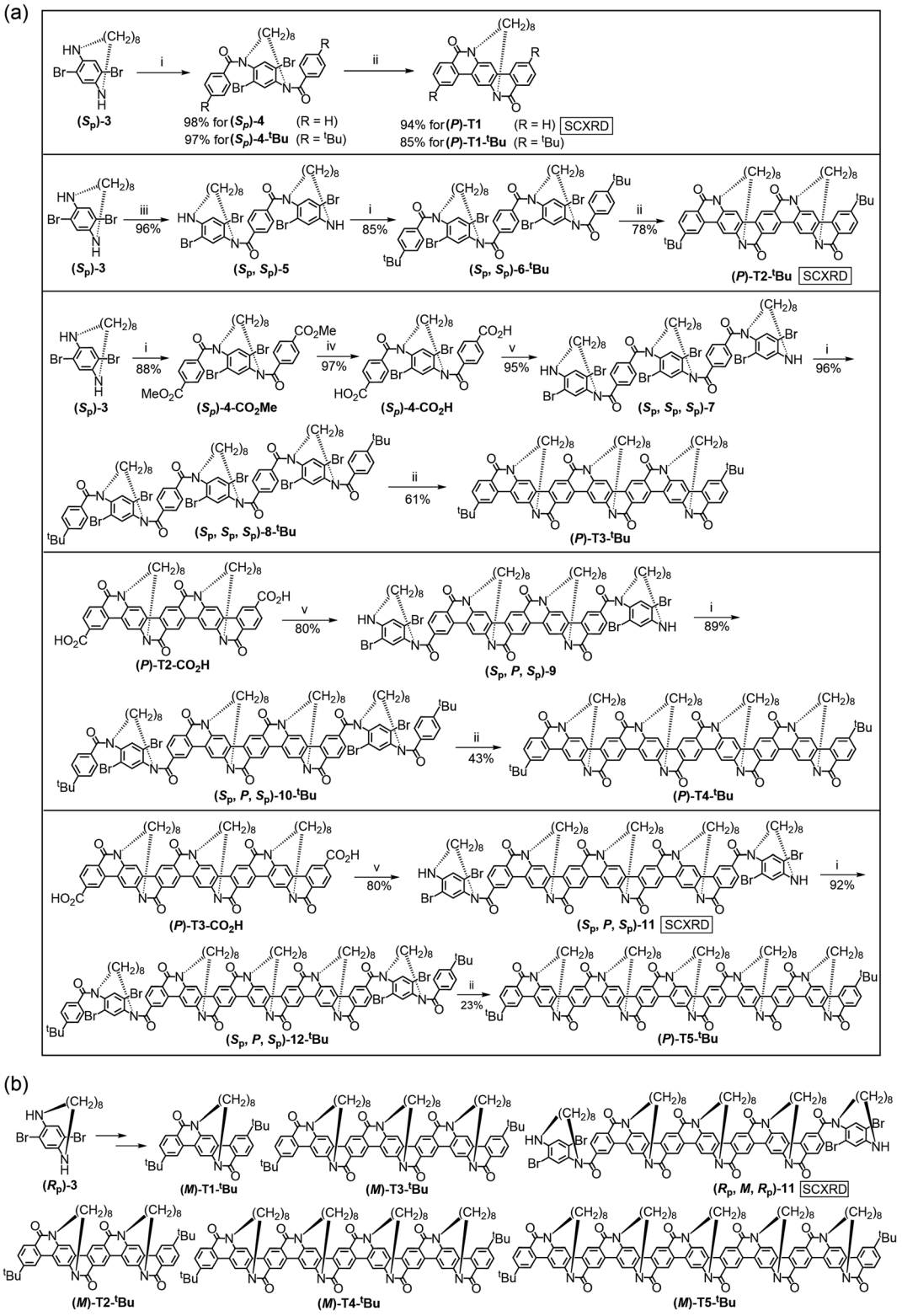

Scheme 2 (a) Synthesis of *P*-chirality concave-type TECHs starting from (S_p)-**3**. (b) Synthesis of *M*-chirality concave-type TECHs starting from (R_p)-**3**. Reaction conditions: (i) Et_3N/ArCOCl, THF, 70 °C; (ii) $Pd(OAc)_2/PCy_3 \cdot HBF_4/Cs_2CO_3$, DMA, 130 °C; (iii) Et_3N/terephthaloyl chloride, CH_2Cl_2, r.t.; (iv) KOH, THF/EtOH/water, 70 °C; (v) 1. oxalyl chloride, CH_2Cl_2, r.t.; 2. Et_3N/(S_p)-**3**, CH_2Cl_2, r.t.

For some compounds, **(*P*)-T1**, **(*P*)-T2-^{t}Bu**, (S_p,*P*,S_p)-11, (R_p,*M*,R_p)-11, and **(*P*)-T2-convex**, their structures and absolute configurations were further determined by SCXRD (*vide infra*). For concave-type TECHs, the intermediates containing amide moieties generally show broadened NMR spectra due to the slow rotation of the amide C–N bond at room temperature.[147–150]

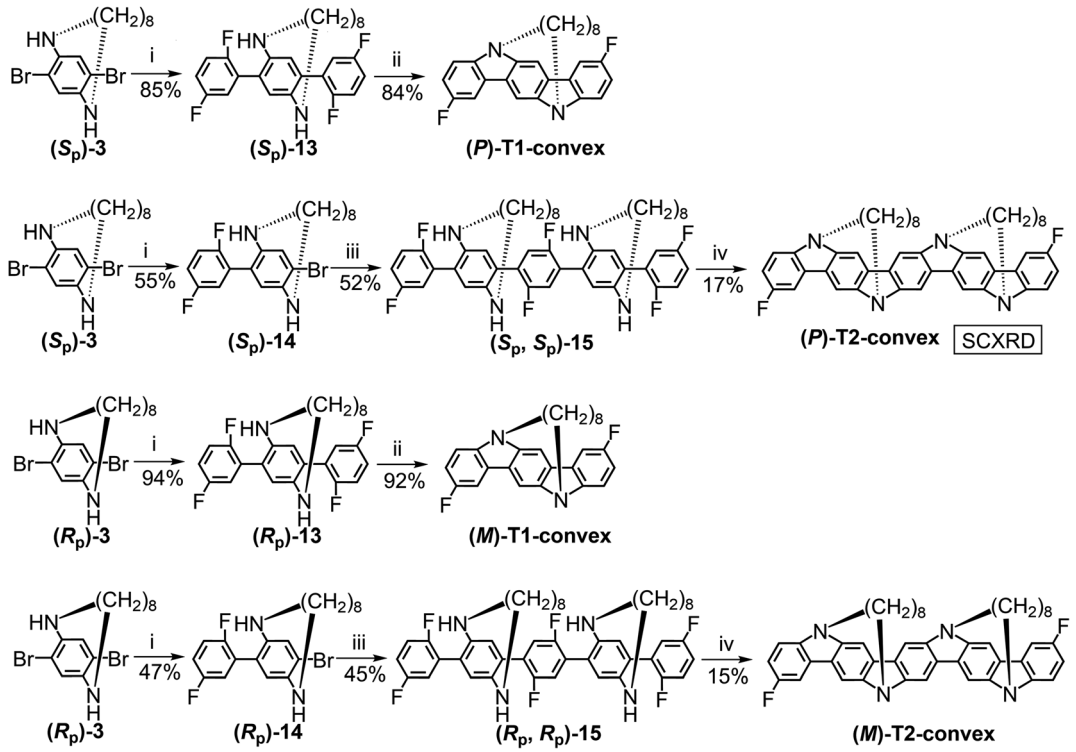

Scheme 3 Synthesis of *P*-chirality and *M*-chirality convex-type TECHs. Reaction conditions: (i) $Pd(PPh_3)_4/K_2CO_3$/2-(2,5-difluorophenyl)-4,4,5,5-tetramethyl-1,3,2-dioxaborolane, THF/water, 70 °C; (ii) KO^{t}Bu, DMF, 80 °C; (iii) $Pd(PPh_3)_4/K_2CO_3$/2,5-difluorobenzene-1,4-diboronicacidbis(pinacol)ester, THF/water, 70 °C; (iv) KO^{t}Bu, DMF, 100 °C.

However, the NMR spectra of the final TECH molecules show sharp signals, suggesting the enhanced molecular rigidity after ladderization. For convex-type TECHs, **(*P*)-T1-convex** and **(*M*)-T1-convex** show sharp signals on NMR, whereas **(*P*)-T2-convex** and **(*M*)-T2-convex** show broadened NMR spectra. This could be due to the lower solubility of **(*P*)-T2-convex** and **(*M*)-T2-convex** in chloroform and the formation of intermolecular aggregates. Both ^{1}H and ^{13}C NMR spectra indicate the C_2 symmetry for all TECH molecules. To further identify the characteristic protons of TECH molecules, 2D-NMR techniques including COSY, NOESY, HSQC, HMBC were employed for **(*P*)-T1-^{t}Bu**, **(*P*)-T2-^{t}Bu**, **(*P*)-T3-^{t}Bu**, **(*P*)-T4-^{t}Bu**, **(*P*)-T5-^{t}Bu**, and **(*P*)-T1-convex** (Fig. S127–S149†). The key correlations and assigned chemical shifts for these compounds are summarized in Fig. S150–S152.† All aromatic protons and partial aliphatic protons were identified. It is noteworthy that all TECH molecules show signals with negative chemical shift on ^{1}H NMR spectra. These signals belong to the central tether protons pointing downward to the benzene ring of the chiral tethering unit. Taking **(*P*)-T1-^{t}Bu** and **(*P*)-T1-convex** for examples, the chemical shifts for the protons are −0.19 and −1.89 ppm, respectively. Since these protons are very close to the benzene rings, the negative chemical shifts could result from the shielding effect of the central aromatic benzene ring. We carried out DFT calculations to verify this hypothesis (Fig. S153†). First, the calculated chemical shifts for all protons of **(*P*)-T1-^{t}Bu** and **(*P*)-T1-convex** are consistent with the experimental ones. The calculated chemical shifts for the tether protons closest to benzene ring are −0.53 and −2.11 ppm for **(*P*)-T1-^{t}Bu** and **(*P*)-T1-convex**, respectively. Second, the nucleus-independent chemical shift (NICS)[151–154] values (*e.g.* NICS(0), NICS(1), and NICS(−1)) indicate the higher aromaticity of the central benzene ring of **(*P*)-T1-convex** than that of **(*P*)-T1-^{t}Bu** (Fig. S153†). The NICS(0), NICS(1), and NICS(−1) values are −7.28, −8.44, and −7.66 ppm for **(*P*)-T1-^{t}Bu**, and −9.78, −11.25, and −8.92 ppm for **(*P*)-T1-convex**, respectively. Therefore, the tether protons above the central benzene of **(*P*)-T1-convex** are more shielded, thus showing a more negative chemical shift. Beside NMR characterization, the HRMS spectra show distinct and expected molecular ion peaks for all TECH molecules (Fig. S154–S170†).

To quantify the chiral strain introduced from tethers, we calculated the strain energy (SE) for all *P*-TECHs by using the homodesmotic reaction method[155–158] (Scheme S4,† Table S1†). The total SE increases along with the number of tethers in either concave-type or convex-type TECHs. The total SE increases from 10.0 kcal mol^{-1} for **(*P*)-T1** to 47.7 kcal mol^{-1} for **(*P*)-T5**, and from 6.5 kcal mol^{-1} for **(*P*)-T1-convex** to 27.9 kcal mol^{-1} for **(*P*)-T5-convex**. On the other hand, the average SE caused by individual tether shows insignificant change for either concave-type or convex-type TECHs. For concave-type TECHs, the SE per tether ranged from 9.5 kcal mol^{-1} to 10.0 kcal mol^{-1}, and for convex-type TECHs, the SE per tether ranged from 5.6 kcal mol^{-1} to 6.5 kcal mol^{-1}. The above results indicate that in a TECH molecule all tethers bend and twist the aromatic backbone with a similar amplitude.

Single crystal structures

Single crystal structures for **(*P*)-T1**, **(*P*)-T2-^{t}Bu**, (S_p,*P*,S_p)-11, (R_p,*M*,R_p)-11, and **(*P*)-T2-convex** are shown in Fig. 3. These structures provide a solid support for the design concept of TECHs. For **(*P*)-T1**, **(*P*)-T2-^{t}Bu**, and (S_p,*P*,S_p)-11 that contain one, two, and three S_p entangling tethers in the ladder aromatic lactam backbone, respectively, all tethers were found in the back of the molecular plane, connecting two adjacent bridge nitrogen atoms from top left to bottom right. The chiral strain induced by these tethers coiled the backbones up into helical ribbons. Viewing along the helical axis, all backbones show the clockwise twist (*P* chirality) and all tethers locate in the outer space of the helical structure. Such concave-type TECH configurations are exactly as what we forecasted in Fig. 1. It was also found that the average bending of the backbone caused by one tether varies in the three molecules. The angles of total bending are ~30°, ~107°, and ~118° for **(*P*)-T1**, **(*P*)-T2-^{t}Bu** and (S_p,*P*,S_p)-11, respectively, corresponding to ~30°, ~54°, and ~39° average bending per tether. This result suggests that although the TECHs are rigid static helical molecules, there is still freedom of motion in bending and twisting, thus rendering them a certain degree of flexibility. For (R_p,*M*,R_p)-11 that with the R_p entangling tethers, it shows a mirror-imaged structure of (S_p,*P*,S_p)-11 and a helical backbone with the anti-clockwise twist (*M* chirality), confirming that the helical chirality of TECHs is only decided by the planar chirality of tethers. Finally, the single crystal structure of **(*P*)-T2-convex** confirmed our prediction about the convex-type TECHs, where the entangling tethers locate in the inner space of the helical structure. The backbone of **(*P*)-T2-convex** is bent by ~56°, corresponding to ~28° average bending per tether. With the S_p entangling tethers, the backbone also shows a *P* chirality.

A more interesting finding is the formation of double-helix dimer in the crystals of concave-type TECHs **(*P*)-T2-^{t}Bu**, (S_p,*P*,S_p)-11, and (R_p,*M*,R_p)-11. As shown in Fig. 4, two molecules of **(*P*)-T2-^{t}Bu** (or (S_p,*P*,S_p)-11, (R_p,*M*,R_p)-11) embrace each other and form a dimer complex *via* the concave face of helical backbone.[159–161] Short center-to-center contacts (*e.g.* 3.42–3.77 Å in **(*P*)-T2-^{t}Bu** dimer, 3.50–3.62 Å in (S_p,*P*,S_p)-11 dimer, 3.57–3.63 Å in (R_p,*M*,R_p)-11 dimer) between the spatially close aromatic rings of two backbones were found for the three dimers. This result suggests that π–π interaction may play an important role in the dimer formation. However, π-dimerization usually takes place between planar conjugated molecules. To verify the unconventional π–π interaction in the double-helix dimers, we carried out DFT calculations for **(*P*)-T2-^{t}Bu** and (S_p,*P*,S_p)-11 dimers. Considering that the terminal groups have little influence to the dimer interactions, we omitted the terminal groups of **(*P*)-T2-^{t}Bu** and (S_p,*P*,S_p)-11 and built up two simplified models named as **(*P*)-T2 dimer** and **(*P*)-T3 dimer**, respectively. The structural optimization was done at the M06-2X(D3)/6-

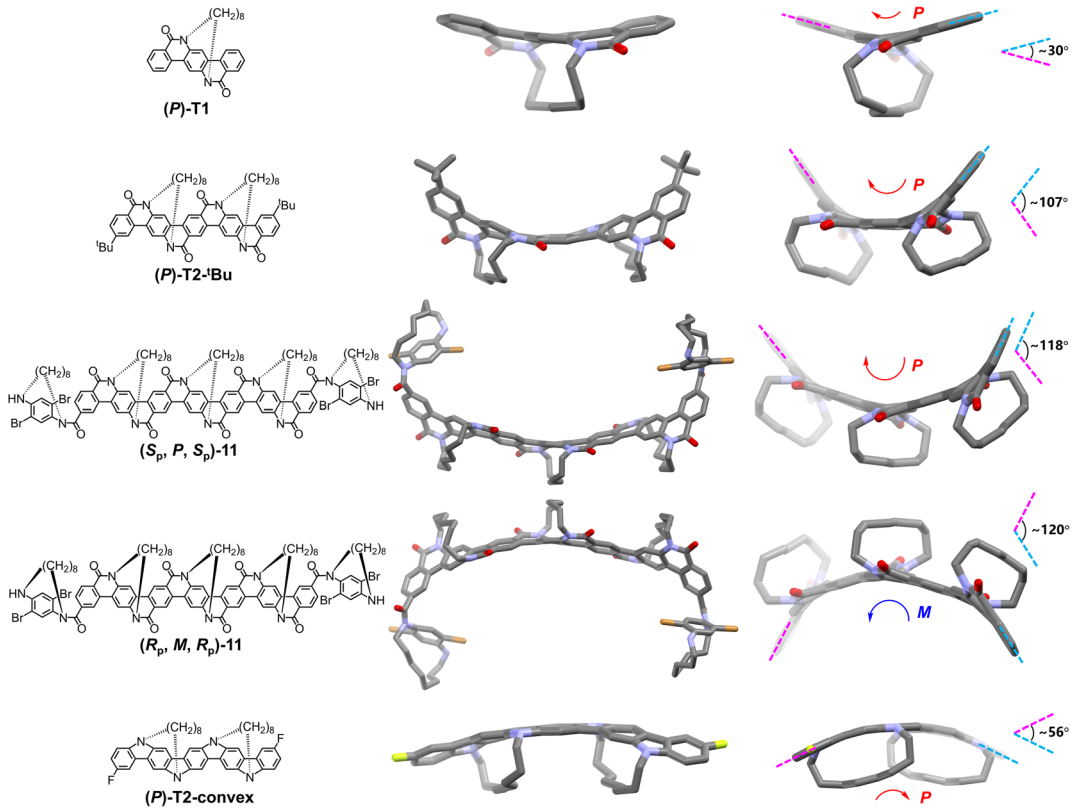

Fig. 3 The chemical structure (left), single crystal structure profile (middle) and the backbone profile viewing along the helical axis (right) for **(*P*)-T1**, **(*P*)-T2-^{t}Bu**, (S_p,*P*,S_p)-11, (R_p,*M*,R_p)-11 and **(*P*)-T2-convex**. Note: hydrogens and solvent molecules in the single crystal structures are omitted for clarity.

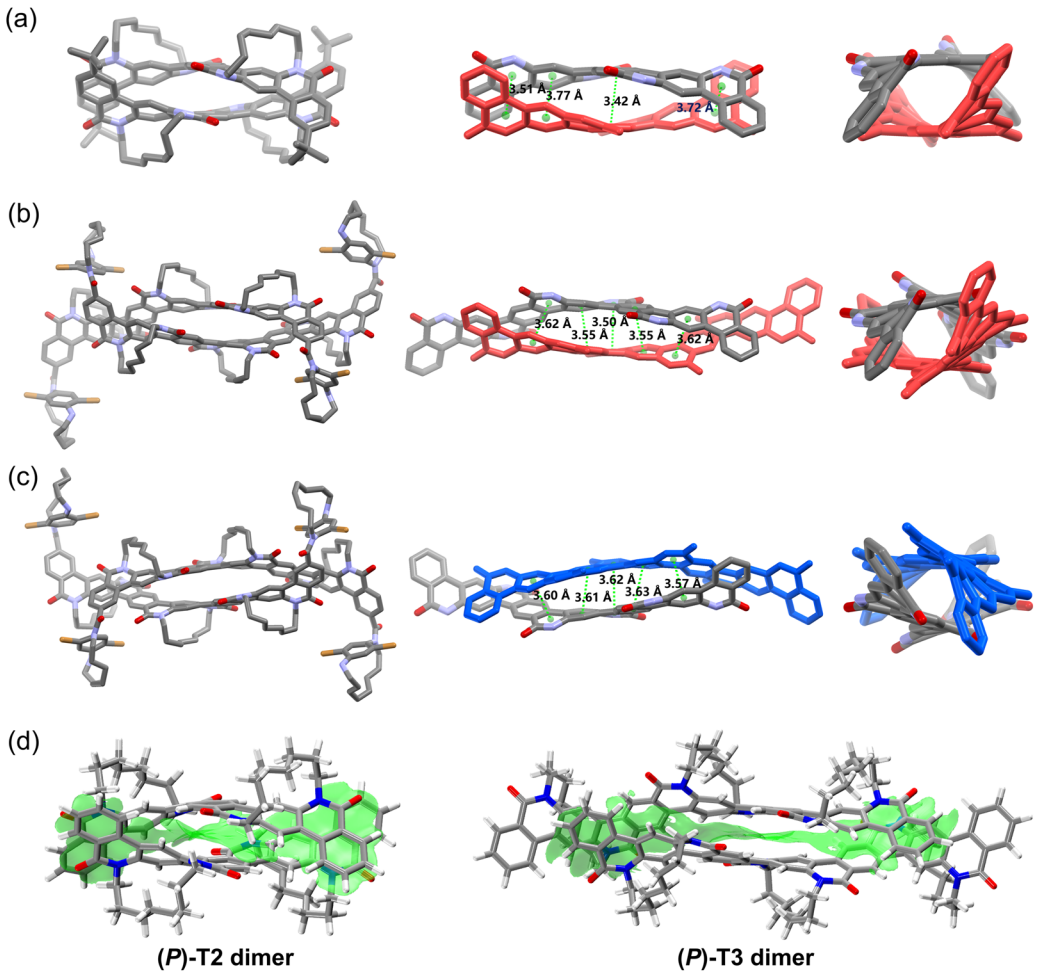

Fig. 4 Double-helix dimers in the crystals of (a) **(*P*)-T2-^{t}Bu**, (b) (S_p,*P*,S_p)-11, and (c) (R_p,*M*,R_p)-11. (d) The DFT-optimized structures and IGMH analysis for **(*P*)-T2 dimer** and **(*P*)-T3 dimer**; the green isosurfaces representing the interfragment interactions were drawn at a δ_g^{inter} value of 0.004.

31G(d,p) level with crystal structure as initial guess. The optimized structures of dimers are shown in Fig. 4d. We conducted independent gradient model based on Hirshfeld partition (IGMH) analysis[162–165] to visualize the real-space noncovalent interactions. It was found that in both dimers a large area of interaction isosurface spreads between the concave π-surfaces of the two monomer fragments, in accordance with the feature of π–π interaction. Moreover, the sandwiched isosurface continuously twists along with the twisted molecular planes. The interaction region indicator (IRI) analysis[166] indicates that the interaction isosurface sandwiched by monomers mainly represents van der Waals attraction (Fig. S171†). The above results verified that considerable π–π interactions exist in the wrapped space of the double-helix dimers and dominate noncovalent interactions. Therefore, they probably provide a driving force for the dimer formation. To get a general understanding of the strength of such unconventional π-dimerization, we investigated the interaction energies (ΔE_{int}) and binding energies (ΔE_b) in **(*P*)-T2 dimer** and **(*P*)-T3 dimer**. For comparison, we also built up two supposititious planar π-dimer models (**planar-T2 dimer** and **planar-T3 dimer**) and calculated ΔE_{int} and ΔE_b in conventional π-dimers (Fig. S172 and S173†). In the case of T2 dimers, the double-helix **(*P*)-T2 dimer** and the **planar-T2 dimer** show comparable ΔE_{int} of −54.4 and −53.6 kcal mol^{-1}, respectively. However, the ΔE_b for **(*P*)-T2 dimer** is apparently smaller than that of **planar-T2 dimer** (−44.7 *vs.* −50.9 kcal mol^{-1}). This is due to the fact that much higher deformation energy (ΔE_d) of 9.7 kcal mol^{-1} should be overcome for the double-helix dimer formation, whereas the ΔE_d for the planar dimer formation is only 2.7 kcal mol^{-1}. The larger ΔE_d for double-helix dimer than planar dimer can be directly visualized from the more obvious structural change of the **(*P*)-T2** monomers before and after dimerization (Fig. S172†). In the case of T3 dimers (Fig. S173†), the double-helix **(*P*)-T3 dimer** not only shows higher ΔE_d than **planar-T3 dimer** (9.5 *vs.* 3.9 kcal mol^{-1}), but also shows smaller ΔE_{int} (−64.5 *vs.* −79.3 kcal mol^{-1}). Thus, the binding energy for **(*P*)-T3 dimer** is much smaller than that of **planar-T3 dimer** (−55.0 *vs.* −75.4 kcal mol^{-1}). From the above, it can be concluded that the tendency for the double-helix π-dimerization is considerably strong, but is not as strong as the conventional planar π-

dimerization, because the monomers have to overcome a larger deformation energy to find a better π–π interaction geometry.

It is worth to note that no double-helix π-dimer is observed in the crystals of **(*P*)-T1** and **(*P*)-T2-convex**. For **(*P*)-T1**, although it belongs to concave-type TECHs, the conjugated backbone is short. Thus, the π–π interaction for **(*P*)-T1** could be relatively weak and may not play a dominate role in molecular aggregation. For **(*P*)-T2-convex**, its concave π-surface is shielded by the entangling tethers. Therefore, the tethers will impede the embracement-like π–π interactions and prevent the formation of dimers. In this regard, only the concave-type TECHs with sufficient backbone length could possess the capability of forming double-helix π-dimers. We envisioned that this capability may be even stronger for longer concave-type TECHs, such as **(*P*)-T4-^{t}Bu** and **(*P*)-T5-^{t}Bu**. Because the crystals of **(*P*)-T4-^{t}Bu** and **(*P*)-T5-^{t}Bu** were not obtained, we investigated their dimer complexes by theoretical calculation. Considering the systems of **(*P*)-T4 dimer** (392 atoms) and **(*P*)-T5 dimer** (484 atoms) are too large, we optimized their structures by using the quantum chemistry program ORCA 5.0.4 at the r^{2}SCAN-3c level.[167–169] The optimized structures of **(*P*)-T4 dimer** and **(*P*)-T5 dimer** as well as the IGMH isosurfaces are shown in Fig. S174.† As expected, both dimers show double-helix geometries and embracement-like π–π interactions. Large ΔE_{int} of −91.5 and −113.7 kcal mol^{-1} were found for **(*P*)-T4 dimer** and **(*P*)-T5 dimer**, respectively.

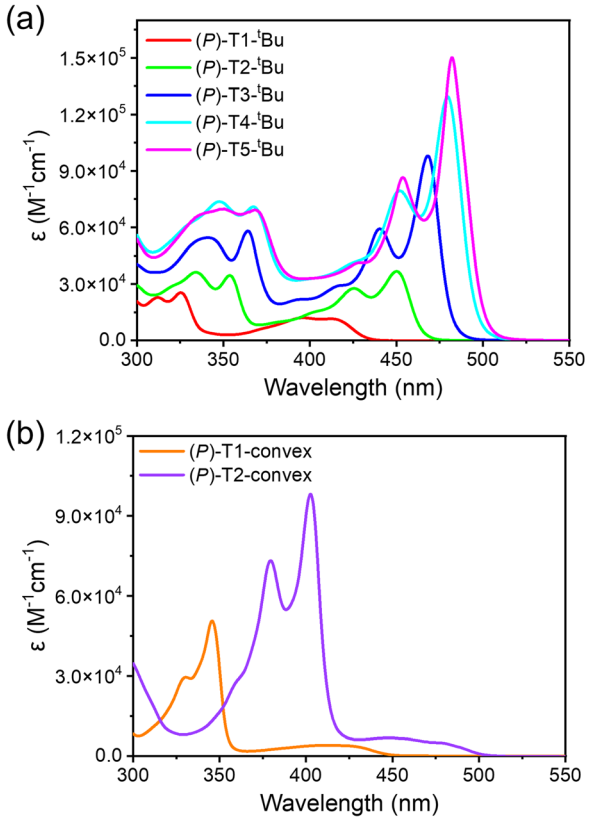

Fig. 5 The absorption spectra for (a) concave-type TECHs and (b) convex-type TECHs in solution. Note: all measurements except that for (*P*)-T5-^{t}Bu were taken in toluene; the measurement for (*P*)-T5-^{t}Bu was taken in toluene : $CHCl_3$ (5 : 1) due to the solubility issue.

Optical and electrochemical properties

The UV-Vis spectra for concave-type and convex-type TECHs are shown in Fig. 5a and b, respectively. Since the *M*-helix TECHs gave identical absorption spectra as their *P*-helix counterparts, only the spectra of *P*-helix TECHs are presented. For concave-type TECHs, all molecules show two major absorption bands. TD-DFT calculations indicate that the low energy band originates from the $S_0 \rightarrow S_1$ electronic transition, whereas the high energy band comes from other higher energy transitions (Fig. S175†). From **(*P*)-T1-^{t}Bu** to **(*P*)-T5-^{t}Bu**, the absorption coefficient of the low energy band increased remarkably due to the significantly enhanced oscillator strength of the $S_0 \rightarrow S_1$ transition. **(*P*)-T5-^{t}Bu** shows the highest molar absorption coefficient of 1.50×10^5 M^{-1} cm^{-1} at 482 nm. For convex-type TECHs, **(*P*)-T1-convex** and **(*P*)-T2-convex** also show two absorption bands. However, due to the low oscillator strength, the $S_0 \rightarrow S_1$ transition bands for **(*P*)-T1-convex** and **(*P*)-T2-convex** are weak and broad. For either concave-type or convex-type TECHs, their absorption spectra show distinct bathochromic shifts as the molecular length increases, indicating that the band gap narrows as the conjugated system elongates. This is similar to the planar ladder-type conjugated molecules. The optical band gaps (E_g^{opt}) were estimated from the absorption onsets. **(*P*)-T1-^{t}Bu**, **(*P*)-T2-^{t}Bu**, **(*P*)-T3-^{t}Bu**, **(*P*)-T4-^{t}Bu**, **(*P*)-T5-^{t}Bu**, **(*P*)-T1-convex** and **(*P*)-T2-convex** show E_g^{opt} of 2.86, 2.67, 2.57, 2.51, 2.48, 2.76, and 2.46 eV, respectively.

The photoluminescence (PL) spectra of TECH molecules are shown in Fig. 6. It was interesting to find that the concave-type TECHs **(*P*)-T2-^{t}Bu**, **(*P*)-T3-^{t}Bu**, **(*P*)-T4-^{t}Bu**, and **(*P*)-T5-^{t}Bu** show distinct concentration-dependent emission behavior, whereas the **(*P*)-T1-^{t}Bu** and the convex-type TECHs **(*P*)-T1-convex** and **(*P*)-T2-convex** do not. At low concentration, the PL spectra of **(*P*)-T2-^{t}Bu** to **(*P*)-T5-^{t}Bu** show clear vibronic progression (*e.g.* the 0-0 and 0-1 transition peaks) and the profiles are mirror images of the $S_0 \rightarrow S_1$ transition band in absorption spectra, indicating that the emission is from the excited single molecules. When concentration increases, the PL maximum shows large bathochromic shifts (29–44 nm) and the vibronic feature disappears. This phenomenon suggests that excimer-like species may form during the luminescence process.[170–173] Reminding that the concave-type TECHs except **(*P*)-T1-^{t}Bu** possess the capability of forming double-helix π-dimers, we considered that the PL at higher concentration is probably from the excited dimers. This is supported by the fact that the PL spectra are similar for the film and high-concentration solution of **(*P*)-T2-^{t}Bu** to **(*P*)-T5-^{t}Bu**.[174–178] We also carried out theoretical calculation to investigate the emission property of monomers and dimers. The calculated fluorescence spectra for **(*P*)-T2**, **(*P*)-T2 dimer**, **(*P*)-T3**, and **(*P*)-T3 dimer** are shown in Fig. 6h. It can be seen that the excited **(*P*)-T2 dimer** and **(*P*)-T3 dimer** show much red-shifted emission than their monomers, supporting the hypothesis that the PL at higher concentration could originate from the excited dimers. The measured PL quantum yields for the dilute solution of TECH molecules are 29%, 43%, 57%, 71%, 46%,

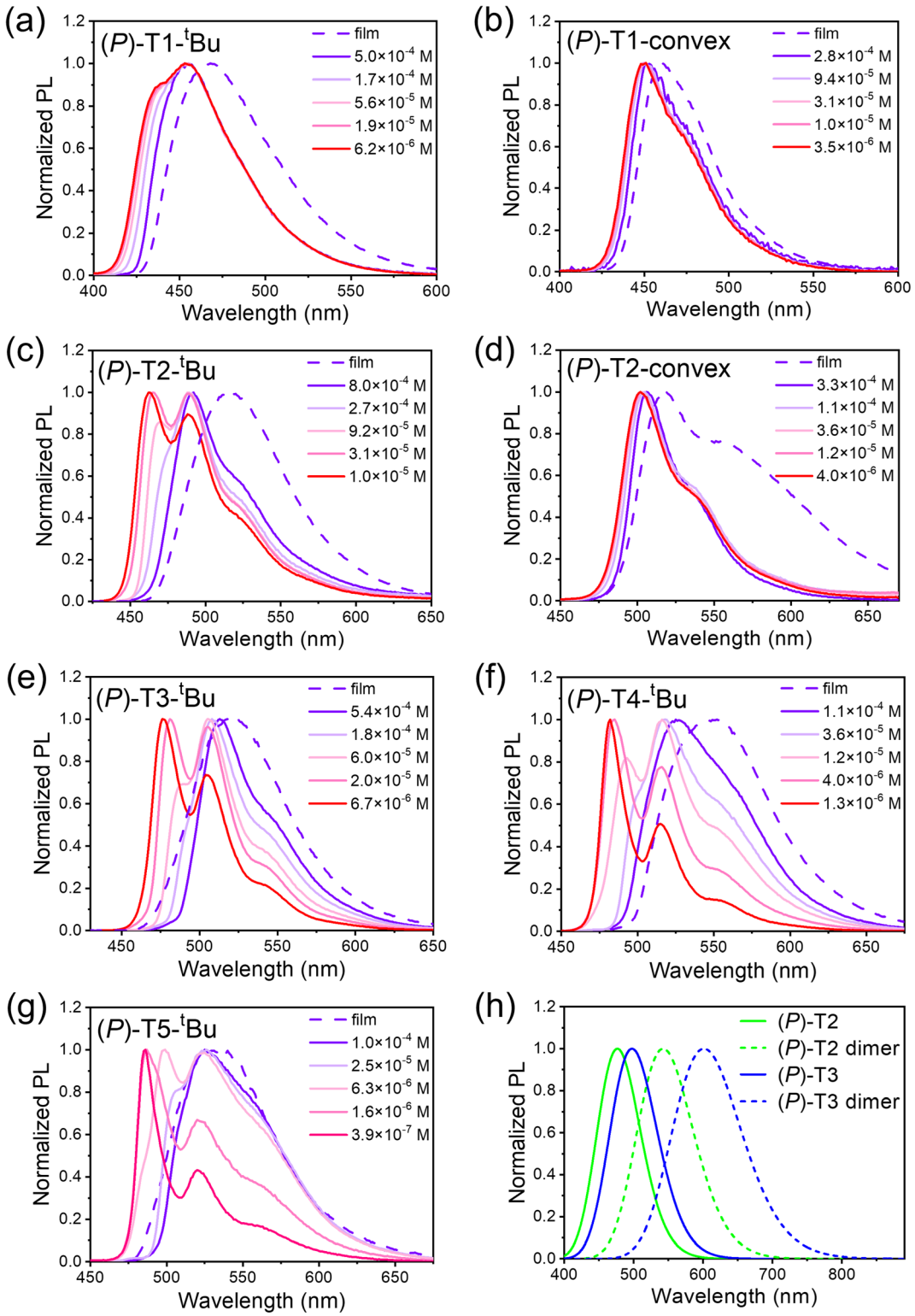

Fig. 6 The photoluminescence spectra for TECHs in solution with different concentration and in film: (a) (*P*)-T1-^{t}Bu; (b) (*P*)-T1-convex; (c) (*P*)-T2-^{t}Bu; (d) (*P*)-T2-convex; (e) (*P*)-T3-^{t}Bu; (f) (*P*)-T4-^{t}Bu; (g) (*P*)-T5-^{t}Bu. (h) The calculated fluorescence spectra for (*P*)-T2, (*P*)-T2 dimer, (*P*)-T3 and (*P*)-T3 dimer by TD-DFT theory at the PBE0(D3)/6-31G(d,p) level.

27%, and 21% for **(*P*)-T1-^{t}Bu**, **(*P*)-T2-^{t}Bu**, **(*P*)-T3-^{t}Bu**, **(*P*)-T4-^{t}Bu**, **(*P*)-T5-^{t}Bu**, **(*P*)-T1-convex**, and **(*P*)-T2-convex**, respectively. The generally higher emission efficiency of concave-type TECHs than convex-type TECHs can be attributed to their stronger oscillator strength of the $S_1 \rightarrow S_0$ transition (Table S2†). For example, the calculated $S_1 \rightarrow S_0$ oscillator strength are 0.18 and 0.70 for **(*P*)-T1** and **(*P*)-T2**, respectively, which are higher than that of their convex counterparts **(*P*)-T1-convex** (0.04) and **(*P*)-**

T2-convex (0.04). In high concentration solution, the PL quantum yields drop for all compounds except (*P*)-**T5-^{t}Bu**. The values are 22%, 36%, 41%, 49%, 50%, 19%, and 12% for (*P*)-**T1-^{t}Bu**, (*P*)-**T2-^{t}Bu**, (*P*)-**T3-^{t}Bu**, (*P*)-**T4-^{t}Bu**, (*P*)-**T5-^{t}Bu**, (*P*)-**T1-convex**, and (*P*)-**T2-convex**, respectively. The decrease of PL quantum yields in high-concentration solution could be due to the aggregation-caused quenching effect. We further conducted time-resolved fluorescence decay measurements for all *P*-TECHs solutions at low or high concentrations (Fig. S176†). It was found that for (*P*)-**T1-^{t}Bu**, (*P*)-**T1-convex**, and (*P*)-**T2-convex** that do not show concentration-dependent emission behavior, only the single-exponential decay was observed, and their low-concentration and high-concentration solutions show similar fluorescence lifetimes. In contrast, (*P*)-**T2-^{t}Bu** to (*P*)-**T5-^{t}Bu** all show bi-exponential decay in the high-concentration solutions, and the ratio of the slow decay component dramatically increased along with concentration. This result suggests that the fast and slow decay components in (*P*)-**T2-^{t}Bu** to (*P*)-**T5-^{t}Bu** could come from the excited monomers and dimers, respectively.

The electrochemical property of TECH molecules was studied by cyclic voltammetry (CV) measurements (Fig. S177†). For all molecules, only oxidation peaks were observed. The concave-type TECHs show higher oxidation potentials than the convex-type TECHs. The HOMO levels calculated from the onset oxidation potentials of (*P*)-**T1-^{t}Bu**, (*P*)-**T2-^{t}Bu**, (*P*)-**T3-^{t}Bu**, (*P*)-**T4-^{t}Bu**, (*P*)-**T5-^{t}Bu**, (*P*)-**T1-convex**, and (*P*)-**T2-convex** are −5.61, −5.59, −5.58, −5.56, −5.55, −5.09, and −4.79 eV, respectively. The deeper HOMO levels of the concave-type TECHs can be attributed to the more electron deficient lactam moieties, which pull down energy levels. The LUMO level was calculated by using HOMO level plus E_g^{opt}. The values are −2.75, −2.92, −3.01, −3.05, −3.07, −2.33, and −2.33 eV, respectively. From (*P*)-**T1-^{t}Bu** to (*P*)-**T5-^{t}Bu**, the elongation of conjugated system of concave-type TECHs leads to slight increase of HOMO level but dramatic decrease of LUMO level. However, in the case of (*P*)-**T1-convex** and (*P*)-**T2-convex**, the elongation of conjugated system majorly lifts up HOMO level and has less influence on LUMO level. The DFT-calculated frontier orbitals and energy levels are shown in Fig. S178.† The theoretically predicted variation trends in HOMO and LUMO levels are consistent with the experimental observations.

Chiroptical properties

Electronic circular dichroism (CD) and CPL tests were carried out for *P*- and *M*-TECHs to investigate their chiral absorption and emission properties. The experimental CD and CPL spectra as well as the theoretical CD spectra for TECHs are shown in Fig. 7. To obtain a good signal to noise ratio on CD spectra, we have to adopt a relatively medium concentration for the test solutions, although there could be co-existed monomers and dimers for the concave-type TECHs. As indicated in Fig. 7, the experimental and theoretical CD spectra have shown good consistency for most of the signals. For all *P*-TECHs, the CD signals close to band gap show negative Cotton effects, which is in good agreement with the theoretical prediction. All *M*-TECHs show mirror-imaged CD spectra as their *P*-counterparts and opposite Cotton effects. For either concave-type or convex-type TECHs, there is an increase tendency in molar circular dichroism ($|\Delta\varepsilon|$) of the near-band gap transitions as the conjugated system elongates. From T1 to T5 concave-type TECHs, the $|\Delta\varepsilon|$ increased from cal. 14 M^{-1} cm^{-1} to cal. 66 M^{-1} cm^{-1}. From T1-convex to T2-convex TECHs, the $|\Delta\varepsilon|$ increases from cal. 6 M^{-1} cm^{-1} to cal. 18 M^{-1} cm^{-1}. On the other hand, the absorption dissymmetry factors (g_{abs}) for the near-band-gap transitions did not show a regular change. For instance, the g_{abs} for (*P*)-**T1-^{t}Bu**, (*P*)-**T2-^{t}Bu**, (*P*)-**T3-^{t}Bu**, (*P*)-**T4-^{t}Bu**, (*P*)-**T5-^{t}Bu**, (*P*)-**T1-convex**, and (*P*)-**T2-convex** are -7.5×10^{-4}, -6.0×10^{-4}, -5.3×10^{-4}, -8.4×10^{-4}, -3.0×10^{-4}, -4.7×10^{-4}, and -5.0×10^{-4}, respectively.

All TECH molecules have exhibited prominent CPL-emission capability. As shown in Fig. 7, *P*- and *M*-TECHs present mirror-imaged CPL spectra, and the signals have the same sign with the corresponding CD signals near the band gap. The CPL shows an increase tendency along with the elongation of conjugated system. The signals increased from cal. 9 mdeg to cal. 58 mdeg for T1 to T5 concave-type TECHs, and from cal. 11 mdeg to cal. 21 mdeg for T1-convex to T2-convex TECHs, respectively. The luminescence dissymmetric factors (g_{lum}) for (*P*)-**T1-^{t}Bu**, (*P*)-**T2-^{t}Bu**, (*P*)-**T3-^{t}Bu**, (*P*)-**T4-^{t}Bu**, (*P*)-**T5-^{t}Bu**, (*P*)-**T1-convex**, and (*P*)-**T2-convex** are -1.1×10^{-3}, -9.2×10^{-4}, -2.6×10^{-3}, -7.0×10^{-3}, -8.1×10^{-3}, -1.4×10^{-3}, and -3.1×10^{-3}, respectively. It is surprising that the *g*-factors are significantly amplified for (*P*)-**T4-^{t}Bu** and (*P*)-**T5-^{t}Bu** during the emission process. The $|g_{lum}|$ are ∼8 and ∼27 folds greater than the $|g_{abs}|$ for (*P*)-**T4-^{t}Bu** and (*P*)-**T5-^{t}Bu**, respectively. For most small molecule chiral emitters, g_{lum} corresponds closely to the g_{abs} near the band gap and usually shows the same magnitude.[179,180] The deviation of $|g_{lum}|$ from $|g_{abs}|$ mainly comes from two possible scenarios: (1) the severe structural change in the excited state *via* vibrational relaxation; (2) the aggregate formation.[180] For rigid aromatic molecules, however, the first circumstance is less possible. We compared the optimized geometries of the ground state and excited state for all *P*-TECHs in Fig. S179.† It was found that the structural change between the two states is insignificant for all compounds. Moreover, the calculated dissymmetric factors g_{abs}^{cal} and g_{lum}^{cal} are close to each other in all cases. Therefore, the relaxation-caused amplification of the dissymmetric factor can be ruled out. Reminding that the concave-type TECHs (*P*)-**T2-^{t}Bu**, (*P*)-**T3-^{t}Bu**, (*P*)-**T4-^{t}Bu**, and (*P*)-**T5-^{t}Bu** exhibited excimer-like emission in high-concentration solutions, we considered that the amplified g_{lum} could be possibly related to aggregation. We investigated the CPL and g_{lum} of all *P*-TECHs at low, medium, and high concentrations (Fig. S180†). The variation of $|g_{lum}|$ along with concentration is summarized in Fig. 8a. It can be seen that (*P*)-**T2-^{t}Bu**, (*P*)-**T3-^{t}Bu**, (*P*)-**T4-^{t}Bu**, and (*P*)-**T5-^{t}Bu** exhibited more pronounced fluctuation of $|g_{lum}|$ along with concentration than the other three TECH molecules. The ratios between the highest and lowest $|g_{lum}|$ for (*P*)-**T2-^{t}Bu**, (*P*)-**T3-^{t}Bu**, (*P*)-**T4-^{t}Bu**, and (*P*)-**T5-^{t}Bu** are 2.8, 4.5, 4.3, and 2.0, respectively, whereas the ratios for (*P*)-**T1-^{t}Bu**, (*P*)-**T1-convex**, and (*P*)-**T2-convex** are close to unity. This suggests aggregation may exist in the concentrated

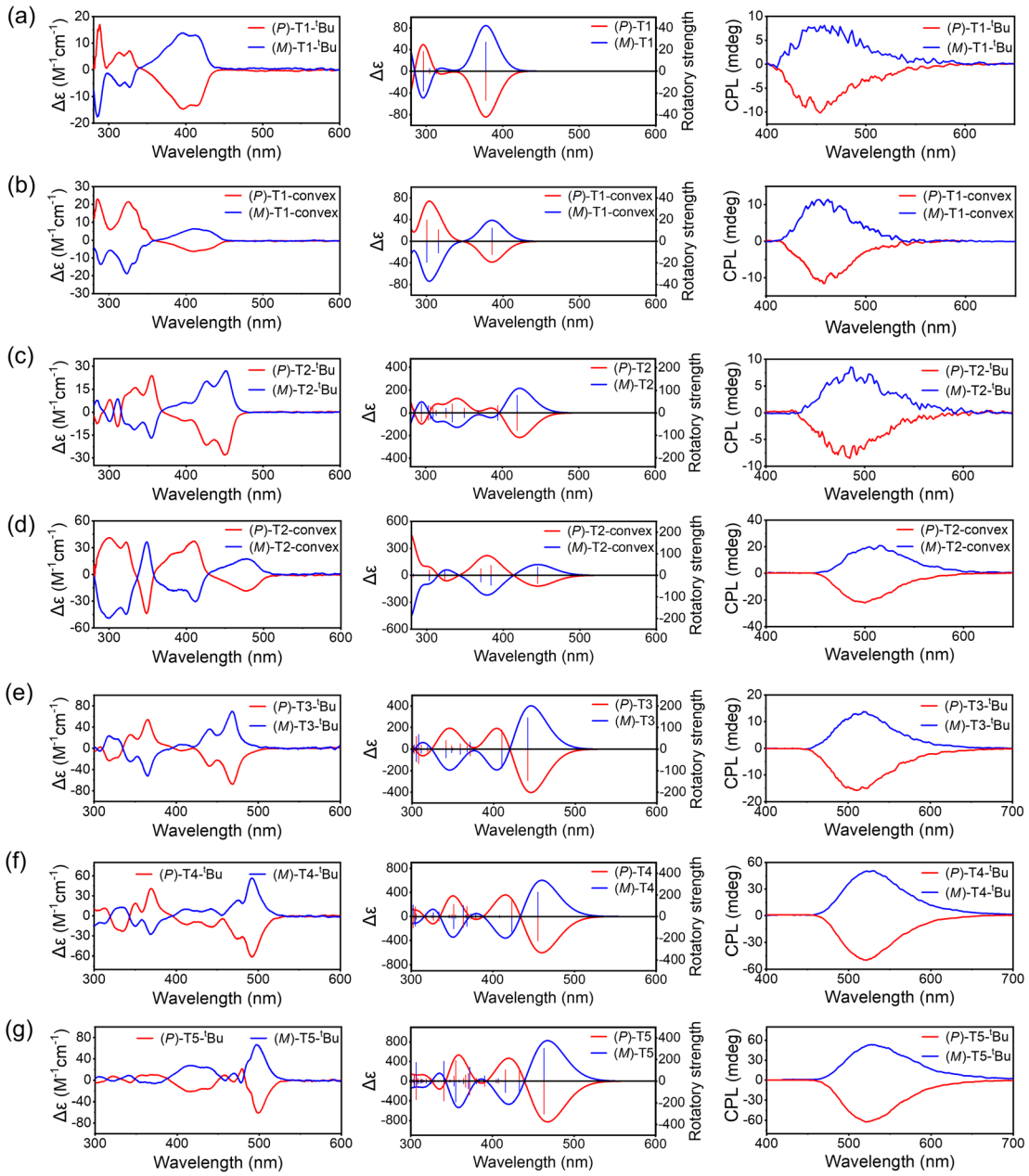

Fig. 7 The experimental CD (left), calculated CD (middle) and experimental CPL (right) spectra for TECHs in solution with a medium concentration: (a) **(*P*)-T1-^{t}Bu** and **(*M*)-T1-^{t}Bu** (5.6×10^{-5} M); (b) **(*P*)-T1-convex** and **(*M*)-T1-convex** (3.1×10^{-5} M); (c) **(*P*)-T2-^{t}Bu** and **(*M*)-T2-^{t}Bu** (9.2×10^{-5} M); (d) **(*P*)-T2-convex** and **(*M*)-T2-convex** (3.6×10^{-5} M); (e) **(*P*)-T3-^{t}Bu** and **(*M*)-T3-^{t}Bu** (6.0×10^{-5} M); (f) **(*P*)-T4-^{t}Bu** and **(*M*)-T4-^{t}Bu** (1.2×10^{-5} M); (g) **(*P*)-T5-^{t}Bu** and **(*M*)-T5-^{t}Bu** (6.3×10^{-6} M).

solutions of **(*P*)-T2-^{t}Bu** to **(*P*)-T5-^{t}Bu**. However, the dynamic light scattering (DLS) measurements indicate that they are all in the molecularly dispersed state with no large aggregates (Fig. S182†). The almost unchanged absorption spectra along with concentration also suggest no obvious aggregation (Fig. S183†). These results support the classic excimer mechanism in the concentrated solutions of **(*P*)-T2-^{t}Bu** to **(*P*)-T5-^{t}Bu**. Thus, in ground state they mainly exist in the form of monomers, but in the excited state they undergo dimerization to form excimers. The $|g_{lum}|$ increment at higher concentrations for **(*P*)-T2-^{t}Bu** to **(*P*)-T5-^{t}Bu** could be caused by the formation of double-helix π-dimers in the excited state. To test the hypothesis, we optimized the geometries of S_1 state of **(*P*)-T2**, **(*P*)-T3** and their dimers **(*P*)-T2 dimer** and **(*P*)-T3 dimer**, and investigated the $S_1 \rightarrow S_0$ transition characteristics (Fig. 8b). In both cases, the $S_1 \rightarrow S_0$ transition characteristics of monomer and dimer are dramatically different. From monomer to dimer, the electric transition dipole moment (μ) decreases by a factor of 4 and 7 for **(*P*)-T2** and **(*P*)-T3**, respectively, whereas the magnetic transition dipole moment (m) increases by a factor of 3 and 17 for **(*P*)-T2** and **(*P*)-T3**, respectively, and the θ between μ and m becomes closer to 180°, thus leading to a great enhancement in the *g*-

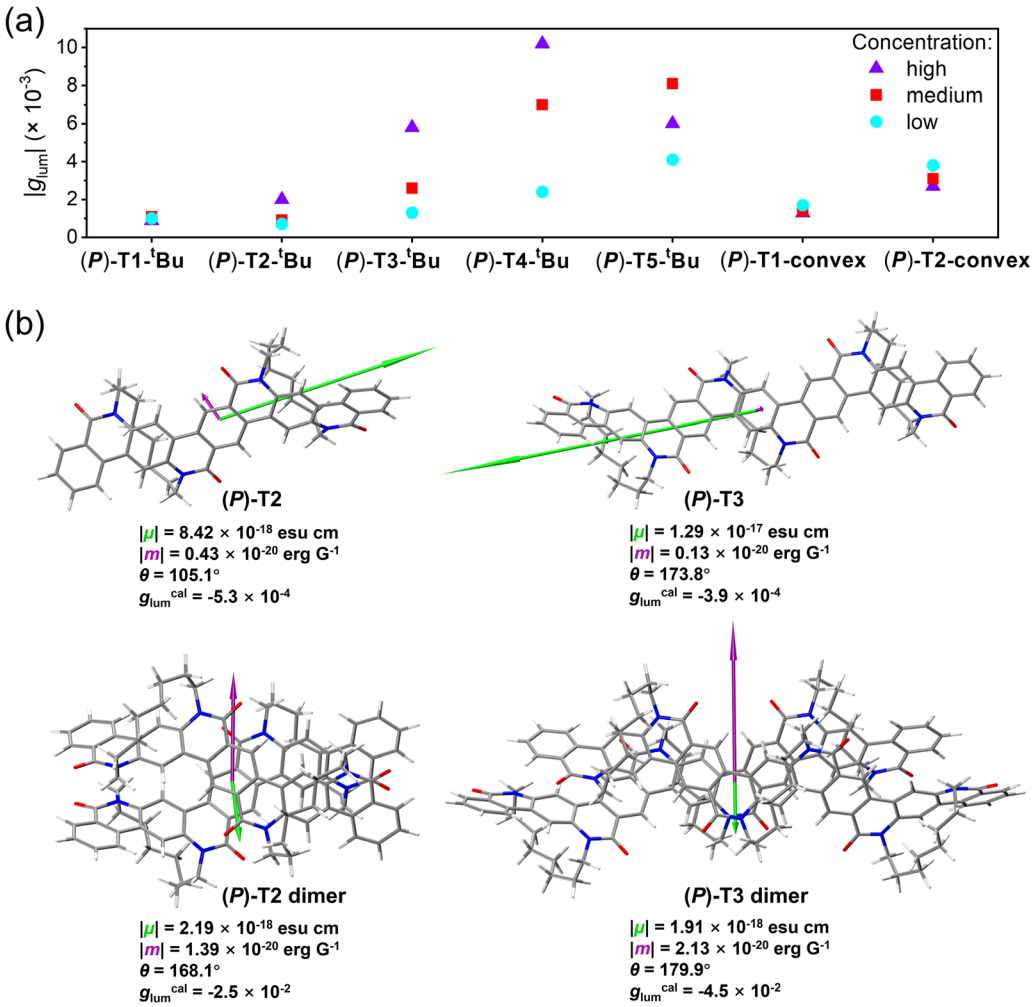

Fig. 8 (a) The variation of $|g_{lum}|$ along with concentration for (*P*)-T1-^{t}Bu, (*P*)-T2-^{t}Bu, (*P*)-T3-^{t}Bu, (*P*)-T4-^{t}Bu, (*P*)-T5-^{t}Bu, (*P*)-T1-convex, and (*P*)-T2-convex. (b) The optimized geometry of S_1 state and the $S_1 \rightarrow S_0$ transition characteristics for (*P*)-T2, (*P*)-T3, (*P*)-T2 dimer, and (*P*)-T3 dimer. Note: the S_1 state geometries were optimized by TD-DFT theory at the PBE0(D3)/6-31G(d,p) level; the *g*-factor was calculated according to the equation $g = 4\cos\theta|m|/|\mu|$, where μ is the electric transition dipole moment, m is the magnetic transition dipole moment, and θ is the angle between μ and m.

factors.[181–184] The g_{lum}^{cal} values for **(*P*)-T2 dimer** and **(*P*)-T3 dimer** are ~45 and ~115 folds higher than those of **(*P*)-T2** and **(*P*)-T3**, respectively. The above theoretical studies support the hypothesis that the double-helix π-dimers in the excited state could make an important contribution in the increased $|g_{lum}|$ for concentrated solutions. It also implies the reason why $|g_{lum}|$ did not change much along with concentration in the case of **(*P*)-T1-^{t}Bu**, **(*P*)-T1-convex**, and **(*P*)-T2-convex** is that these molecules do not have the capability of forming double-helix π-dimers. It is worth to note that the $|g_{lum}|$ of **(*P*)-T4-^{t}Bu** in high-concentration solution reached 1.0×10^{-2}, which is a considerably high value for organic chiral emitters in solution. The $|g_{lum}|$ values for ordinary small molecule chiral emitters are usually around 10^{-4} to 10^{-3}.[185–189] Reminding that **(*P*)-T4-^{t}Bu** also shows a relatively high PL quantum yield (71% in dilute solution, 49% in high-concentration solution) and a high molar absorption coefficient (1.29×10^5 M^{-1} cm^{-1} at 480 nm), **(*P*)-T4-^{t}Bu** possesses a high CPL brightness[179] of 316 M^{-1} cm^{-1} (110 M^{-1} cm^{-1} in dilute solution), which is among the best values for organic chiral emitters to date.[190–194]

At last, we investigated the chiroptical stability of TECHs. Traditional optically pure helical polyaromatic molecules like helicenes and twistacenes can lose their optical activity due to the surmountable racemization barriers. However, the racemization for TECHs is almost impossible because the helical configuration is covalently locked by the entangling tethers.[159,195–207] Therefore, the TECH molecules will never lose their chiroptical properties unless the entangling tethers are cleaved. After heating all *P*- and *M*-TECHs in toluene at 100 °C for 24 h, we found that the CD spectra did not show any decay of signals for all compounds, thus demonstrating the excellent configurational and chiroptical stability of TECHs (Fig. S184†).

Conclusions

In summary, we have introduced a new TECH concept for helical polyaromatic molecules. Different from traditional

helicenes and twistacenes, the helical structures of TECHs are no longer decided by the steric effect but by the chiral strain induced from the entangling tethers. TECHs can be directly constructed in enantiopure form *via* modular synthesis to have unique 3D features. Moreover, the covalent locking of helical configuration by tethers renders them stable and persistent chiral properties. Guided by this concept, we successfully prepared the concave-type and convex-type oligomeric TECHs. The crystal structures of these molecules not only proved the validity and feasibility of the TECH principle, but also unveiled an interesting double-helix π-dimerization behavior of the concave-type TECHs. Prominent and persistent chiroptical properties were observed for all TECH molecules. The **(*P*)-T4-^{t}Bu** demonstrated the highest $|g_{lum}|$ of 1.0×10^{-2} and an impressive CPL brightness of 316 M^{-1} cm^{-1}. It is expected that by further modifying the chiral tethering units and docking units, more TECH molecules with diverse 3D helical geometries (*e.g.* different lengths, diameters, and pitches) can be created. With novel and tunable helical architectures and robust chiral properties, TECHs may find interesting applications in the future. Efforts on the synthesis of polymeric TECHs and the exploration of applications are currently under way.

Data availability

The data that support the findings of this study are available from the corresponding author upon reasonable request.

Author contributions

K. J. and Z. X. conceptualized the work. K. J. and H. X. synthesized the compounds. K. J. performed the characterization and property tests of the compounds. K. J. and Z. X. conducted data analysis. X. S. performed theoretical calculations. J. W., X. C., Z. W., Z. Z., K. Y. and Y. D. directed the experiments and discussed the results. Z. X. and L. D. directed the project and wrote the manuscript.

Conflicts of interest

The authors declare no conflict of interest.

Acknowledgements

The authors thank the National Key Research and Development Program of China (2022YFB3803300, 2023YFE0116800), Beijing Natural Science Foundation (IS23037) and the Strategic Priority Research Program of Chinese Academy of Sciences (XDB36000000) for financial support. This work is supported by High Performance Computing Center of NCNST, China.

References

1 Y. Shen and C. F. Chen, Helicenes: synthesis and applications, *Chem. Rev.*, 2012, **112**, 1463–1535.
2 D. W. Zhang, M. Li and C. F. Chen, Recent advances in circularly polarized electroluminescence based on organic light-emitting diodes, *Chem. Soc. Rev.*, 2020, **49**, 1331–1343.
3 H. V. Anderson, N. D. Gois and W. A. Chalifoux, New advances in chiral nanographene chemistry, *Org. Chem. Front.*, 2023, **10**, 4167–4197.
4 Y. Zhu and J. Wang, Helical Synthetic Nanographenes with Atomic Precision, *Acc. Chem. Res.*, 2023, **56**, 363–373.
5 Y. Yang, R. C. da Costa, M. J. Fuchter and A. J. Campbell, Circularly polarized light detection by a chiral organic semiconductor transistor, *Nat. Photonics*, 2013, **7**, 634–638.
6 J. Schummer, Molecular Aesthetics: Blind Alleys and Fertile Soils, In *Molecular Aesthetics*, ed. P. Weibel and Lj. Fruk, MIT Press, Cambridge, MA, 2013, pp. 155–161.
7 L. Zhang, I. Song, J. Ahn, M. Han, M. Linares, M. Surin, H. J. Zhang, J. H. Oh and J. Lin, π-Extended perylene diimide double-heterohelicenes as ambipolar organic semiconductors for broadband circularly polarized light detection, *Nat. Commun.*, 2021, **12**, 142.
8 D. Zhu, W. Jiang, Z. Ma, J. Feng, X. Zhan, C. Lu, J. Liu, J. Liu, Y. Hu, D. Wang, Y. S. Zhao, J. Wang, Z. Wang and L. Jiang, Organic donor-acceptor heterojunctions for high performance circularly polarized light detection, *Nat. Commun.*, 2022, **13**, 3454.
9 D. Meng, H. Fu, C. Xiao, X. Meng, T. Winands, W. Ma, W. Wei, B. Fan, L. Huo, N. L. Doltsinis, Y. Li, Y. Sun and Z. Wang, Three-Bladed Rylene Propellers with Three-Dimensional Network Assembly for Organic Electronics, *J. Am. Chem. Soc.*, 2016, **138**, 10184–10190.
10 S. Rasool, J. Yeop, H. W. Cho, W. Lee, J. W. Kim, D. Yuk and J. Y. Kim, Path to the fabrication of efficient, stable and commercially viable large-area organic solar cells, *Mater. Futures*, 2023, **2**, 032102.
11 C. Gedeon, N. Del Rio, F. Furlan, A. Taddeucci, N. Vanthuyne, V. G. Gregoriou, M. J. Fuchter, G. Siligardi, N. Gasparini, J. Crassous and C. L. Chochos, Rational Design of New Conjugated Polymers with Main Chain Chirality for Efficient Optoelectronic Devices: Carbo[6] Helicene and Indacenodithiophene Copolymers as Model Compounds, *Adv. Mater.*, 2024, **36**, e2314337.
12 V. Kiran, S. P. Mathew, S. R. Cohen, I. Hernández Delgado, J. Lacour and R. Naaman, Helicenes—A New Class of Organic Spin Filter, *Adv. Mater.*, 2016, **28**, 1957–1962.
13 M. Rickhaus, M. Mayor and M. Juríček, Strain-induced helical chirality in polyaromatic systems, *Chem. Soc. Rev.*, 2016, **45**, 1542–1556.
14 R. Rodríguez, C. Naranjo, A. Kumar, P. Matozzo, T. K. Das, Q. Zhu, N. Vanthuyne, R. Gomez, R. Naaman, L. Sánchez and J. Crassous, Mutual Monomer Orientation To Bias the Supramolecular Polymerization of [6]Helicenes and the Resulting Circularly Polarized Light and Spin Filtering Properties, *J. Am. Chem. Soc.*, 2022, **144**, 7709–7719.
15 Q. Yan, S. Tao, R. Liu, Y. Zhi and D. Jiang, Crystalline, Porous Helicene Covalent Organic Frameworks, *Angew Chem. Int. Ed. Engl.*, 2024, **63**, e202316092.
16 W. C. Guo, W. L. Zhao, K. K. Tan, M. Li and C. F. Chen, B,N-Embedded Hetero[9]helicene Toward Highly Efficient

Circularly Polarized Electroluminescence, *Angew Chem. Int. Ed. Engl.*, 2024, **63**, e202401835.
17 J. Wade, F. Salerno, R. C. Kilbride, D. K. Kim, J. A. Schmidt, J. A. Smith, L. M. LeBlanc, E. H. Wolpert, A. A. Adeleke, E. R. Johnson, J. Nelson, T. Mori, K. E. Jelfs, S. Heutz and M. J. Fuchter, Controlling anisotropic properties by manipulating the orientation of chiral small molecules, *Nat. Chem.*, 2022, **14**, 1383–1389.
18 C. F. Chen and Y. Shen, In *Helicene Chemistry: From Synthesis to Applications*, Springer, Berlin, Heidelberg, 2017, pp. 1–272.
19 K. K. Wang, Twisted Arenes, *Top. Curr. Chem.*, 2012, **349**, 31–61.
20 W. H. Laarhoven and W. J. C. Prinsen, Carbohelicenes and heterohelicenes, *Top. Curr. Chem.*, 1984, **125**, 63–130.
21 K. P. Meurer and F. Vögtle, Helical Molecules in Organic Chemistry, *Top. Curr. Chem.*, 1985, **127**, 1–76.
22 R. Weitzenböck and A. Klingler, A. Synthese der isomeren Kohlenwasserstoffe 1, 2–5, 6-Dibenzanthracen und 3, 4–5, 6-Dibenzphenanthren, *Monatsh. Chem.*, 1918, **39**, 315–323.
23 M. S. Newman and D. Lednicer, The Synthesis and Resolution of Hexahelicene, *J. Am. Chem. Soc.*, 1956, **78**, 4765–4770.
24 M. Flammand-Barbieux, J. Nasielski and R. H. Martin, Synthesis of heptahelicene (1) benzo [c] phenanthro [4,3-g]phenanthrene, *Tetrahedron Lett.*, 1967, **7**, 743–744.
25 M. Gingras, One hundred years of helicene chemistry. Part 1: non-stereoselective syntheses of carbohelicenes, *Chem. Soc. Rev.*, 2013, **42**, 968–1006.
26 M. Gingras, G. Felix and R. Peresutti, One hundred years of helicene chemistry. Part 2: stereoselective syntheses and chiral separations of carbohelicenes, *Chem. Soc. Rev.*, 2013, **42**, 1007–1050.
27 M. Gingras, One hundred years of helicene chemistry. Part 3: applications and properties of carbohelicenes, *Chem. Soc. Rev.*, 2013, **42**, 1051–1095.
28 L. J. Peng, X. Y. Wang, Z. A. Li and H. Y. Gong, All Carbon Helicenes and π-Extended Helicene Derivatives, *Asian J. Org. Chem.*, 2023, **12**, e202300543.
29 K. Dhbaibi, L. Favereau and J. Crassous, Enantioenriched Helicenes and Helicenoids Containing Main-Group Elements (B, Si, N, P), *Chem. Rev.*, 2019, **119**, 8846–8953.
30 W. W. Yang and J. J. Shen, Multiple Heterohelicenes: Synthesis, Properties and Applications, *Chem.–Eur. J.*, 2022, **28**, e202202069.
31 A. Rajca, M. Miyasaka, M. Pink, H. Wang and S. Rajca, Helically Annelated and Cross-Conjugated Oligothiophenes: Asymmetric Synthesis, Resolution, and Characterization of a Carbon-Sulfur [7]Helicene, *J. Am. Chem. Soc.*, 2004, **126**, 15211–15222.
32 K. Yavari, S. Moussa, B. Ben Hassine, P. Retailleau, A. Voituriez and A. Marinetti, 1*H*-phosphindoles as structural units in the synthesis of chiral helicenes, *Angew Chem. Int. Ed. Engl.*, 2012, **51**, 6748–6752.
33 K. Nakano, H. Oyama, Y. Nishimura, S. Nakasako and K. Nozaki, λ^5-Phospha[7]helicenes: synthesis, properties, and columnar aggregation with one-way chirality, *Angew Chem. Int. Ed. Engl.*, 2012, **51**, 695–699.
34 T. Shibata, T. Uchiyama, Y. Yoshinami, S. Takayasu, K. Tsuchikama and K. Endo, Highly enantioselective synthesis of silahelicenes using Ir-catalyzed [2+2+2] cycloaddition, *Chem. Commun.*, 2012, **48**, 1311–1313.
35 H. Oyama, K. Nakano, T. Harada, R. Kuroda, M. Naito, K. Nobusawa and K. Nozaki, Facile Synthetic Route to Highly Luminescent Sila[7]helicene, *Org. Lett.*, 2013, **15**, 2104–2107.
36 S. Oda, B. Kawakami, Y. Yamasaki, R. Matsumoto, M. Yoshioka, D. Fukushima, S. Nakatsuka and T. Hatakeyama, One-Shot Synthesis of Expanded Heterohelicene Exhibiting Narrowband Thermally Activated Delayed Fluorescence, *J. Am. Chem. Soc.*, 2022, **144**, 106–112.
37 J. K. Li, X. Y. Chen, Y. L. Guo, X. C. Wang, A. C. Sue, X. Y. Cao and X. Y. Wang, B,N-Embedded Double Hetero[7]helicenes with Strong Chiroptical Responses in the Visible Light Region, *J. Am. Chem. Soc.*, 2021, **143**, 17958–17963.
38 C. Qu, Y. Xu, Y. Wang, Y. Nie, K. Ye, H. Zhang and Z. Zhang, Bridging of Cove Regions: A Strategy for Realizing Persistently Chiral Double Heterohelicenes with Attractive Luminescent Properties, *Angew Chem. Int. Ed. Engl.*, 2024, **63**, e202400661.
39 Z. Sun, W. Xu, S. Qiu, Z. Ma, C. Li, S. Zhang and H. Wang, Thia[*n*]helicenes with long persistent phosphorescence, *Chem. Sci.*, 2024, **15**, 1077–1087.
40 N. Saleh, C. Shen and J. Crassous, Helicene-based transition metal complexes: synthesis, properties and applications, *Chem. Sci.*, 2014, **5**, 3680–3694.
41 E. S. Gauthier, R. Rodríguez and J. Crassous, Metal-Based Multihelicenic Architectures, *Angew Chem. Int. Ed. Engl.*, 2020, **59**, 22840–22856.
42 L. Norel, M. Rudolph, N. Vanthuyne, J. A. Williams, C. Lescop, C. Roussel, J. Autschbach, J. Crassous and R. Reau, Metallahelicenes: easily accessible helicene derivatives with large and tunable chiroptical properties, *Angew Chem. Int. Ed. Engl.*, 2010, **49**, 99–102.
43 S. Graule, M. Rudolph, W. Shen, J. A. Williams, C. Lescop, J. Autschbach, J. Crassous and R. Reau, Assembly of π-conjugated phosphole azahelicene derivatives into chiral coordination complexes: an experimental and theoretical study, *Chem.–Eur. J.*, 2010, **16**, 5976–6005.
44 V. Vreshch, M. El Sayed Moussa, B. Nohra, M. Srebro, N. Vanthuyne, C. Roussel, J. Autschbach, J. Crassous, C. Lescop and R. Reau, Assembly of helicene-capped N,P,N,P,N-helicands within Cu(I) helicates: impacting chiroptical properties by ligand-ligand charge transfer, *Angew Chem. Int. Ed. Engl.*, 2013, **52**, 1968–1972.
45 J. R. Brandt, X. Wang, Y. Yang, A. J. Campbell and M. J. Fuchter, Circularly Polarized Phosphorescent Electroluminescence with a High Dissymmetry Factor from PHOLEDs Based on a Platinahelicene, *J. Am. Chem. Soc.*, 2016, **138**, 9743–9746.

46 W.-B. Lin, M. Li, L. Fang and C.-F. Chen, Recent progress on multidimensional construction of helicenes, *Chin. Chem. Lett.*, 2018, **29**, 40–46.
47 K. Kato, Y. Segawa and K. Itami, Symmetric Multiple Carbohelicenes, *Synlett*, 2018, **30**, 370–377.
48 Y.-F. Wu, L. Zhang, Q. Zhang, S.-Y. Xie and L.-S. Zheng, Multiple [*n*]helicenes with various aromatic cores, *Org. Chem. Front.*, 2022, **9**, 4726–4743.
49 T. Mori, Chiroptical Properties of Symmetric Double, Triple, and Multiple Helicenes, *Chem. Rev.*, 2021, **121**, 2373–2412.
50 T. Fujikawa, Y. Segawa and K. Itami, Synthesis and Structural Features of Quadruple Helicenes: Highly Distorted pi Systems Enabled by Accumulation of Helical Repulsions, *J. Am. Chem. Soc.*, 2016, **138**, 3587–3595.
51 T. Hosokawa, Y. Takahashi, T. Matsushima, S. Watanabe, S. Kikkawa, I. Azumaya, A. Tsurusaki and K. Kamikawa, Synthesis, Structures, and Properties of Hexapole Helicenes: Assembling Six [5]Helicene Substructures into Highly Twisted Aromatic Systems, *J. Am. Chem. Soc.*, 2017, **139**, 18512–18521.
52 B. Liu, M. Bockmann, W. Jiang, N. L. Doltsinis and Z. Wang, Perylene Diimide-Embedded Double [8]Helicenes, *J. Am. Chem. Soc.*, 2020, **142**, 7092–7099.
53 Y. Chen, C. Lin, Z. Luo, Z. Yin, H. Shi, Y. Zhu and J. Wang, Double π-Extended Undecabenzo[7]helicene, *Angew Chem. Int. Ed. Engl.*, 2021, **60**, 7796–7801.
54 W. Niu, Y. Fu, Q. Deng, Z. L. Qiu, F. Liu, A. A. Popov, H. Komber, J. Ma and X. Feng, Enhancing Chiroptical Responses in Helical Nanographenes via Geometric Engineering of Double [7]Helicenes, *Angew Chem. Int. Ed. Engl.*, 2024, **63**, e202319874.
55 P. J. Evans, J. Ouyang, L. Favereau, J. Crassous, I. Fernández, J. Perles and N. Martin, Synthesis of a Helical Bilayer Nanographene, *Angew Chem. Int. Ed. Engl.*, 2018, **57**, 6774–6779.
56 Y. Nakakuki, T. Hirose, H. Sotome, H. Miyasaka and K. Matsuda, Hexa- peri-hexabenzo[7]helicene: Homogeneously π-Extended Helicene as a Primary Substructure of Helically Twisted Chiral Graphenes, *J. Am. Chem. Soc.*, 2018, **140**, 4317–4326.
57 J. Ma, Y. Fu, E. Dmitrieva, F. Liu, H. Komber, F. Hennersdorf, A. A. Popov, J. J. Weigand, J. Liu and X. Feng, Helical Nanographenes Containing an Azulene Unit: Synthesis, Crystal Structures, and Properties, *Angew Chem. Int. Ed. Engl.*, 2020, **59**, 5637–5642.
58 X. Xiao, S. K. Pedersen, D. Aranda, J. Yang, R. A. Wiscons, M. Pittelkow, M. L. Steigerwald, F. Santoro, N. J. Schuster and C. Nuckolls, Chirality Amplified: Long, Discrete Helicene Nanoribbons, *J. Am. Chem. Soc.*, 2021, **143**, 983–991.
59 Y. Nakakuki, T. Hirose, H. Sotome, M. Gao, D. Shimizu, R. Li, J. Y. Hasegawa, H. Miyasaka and K. Matsuda, Doubly linked chiral phenanthrene oligomers for homogeneously π-extended helicenes with large effective conjugation length, *Nat. Commun.*, 2022, **13**, 1475.
60 G. R. Kiel, H. M. Bergman, A. E. Samkian, N. J. Schuster, R. C. Handford, A. J. Rothenberger, R. Gomez-Bombarelli, C. Nuckolls and T. D. Tilley, Expanded [23]-Helicene with Exceptional Chiroptical Properties via an Iterative Ring-Fusion Strategy, *J. Am. Chem. Soc.*, 2022, **144**, 23421–23427.
61 J. K. Li, X. Y. Chen, W. L. Zhao, Y. L. Guo, Y. Zhang, X. C. Wang, A. C. Sue, X. Y. Cao, M. Li, C. F. Chen and X. Y. Wang, Synthesis of Highly Luminescent Chiral Nanographene, *Angew Chem. Int. Ed. Engl.*, 2023, **62**, e202215367.
62 X. Tian, K. Shoyama, B. Mahlmeister, F. Brust, M. Stolte and F. Würthner, Naphthalimide-Annulated [*n*]Helicenes: Red Circularly Polarized Light Emitters, *J. Am. Chem. Soc.*, 2023, **145**, 9886–9894.
63 G. F. Huo, T. M. Fukunaga, X. Hou, Y. Han, W. Fan, S. Wu, H. Isobe and J. Wu, Facile Synthesis and Chiral Resolution of Expanded Helicenes with up to 35 cata-Fused Benzene Rings, *Angew Chem. Int. Ed. Engl.*, 2023, **62**, e202218090.
64 F. Morita, Y. Kishida, Y. Sato, H. Sugiyama, M. Abekura, J. Nogami, N. Toriumi, Y. Nagashima, T. Kinoshita, G. Fukuhara, M. Uchiyama, H. Uekusa and K. Tanaka, Design and enantioselective synthesis of 3D π-extended carbohelicenes for circularly polarized luminescence, *Nat. Synth.*, 2024, **3**, 774–786.
65 R. A. Pascal, Twisted acenes, *Chem. Rev.*, 2006, **106**, 4809–4819.
66 R. A. Pascal, W. D. McMillan, D. Van Engen and R. G. Eason, Synthesis and structure of longitudinally twisted polycyclic aromatic hydrocarbons, *J. Am. Chem. Soc.*, 1987, **109**, 4660–4665.
67 N. Smyth, D. Van Engen and R. A. Pascal, Synthesis of longitudinally twisted polycyclic aromatic hydrocarbons via a highly substituted aryne, *J. Org. Chem.*, 1990, **55**, 1937–1940.
68 X. Qiao, D. M. Ho and R. A. Pascal, An Extraordinarily Twisted Polycyclic Aromatic Hydrocarbon, *Angew Chem. Int. Ed. Engl.*, 2003, **36**, 1531–1532.
69 J. Lu, D. M. Ho, N. J. Vogelaar, C. M. Kraml and R. A. Pascal, A Pentacene with a 144° Twist, *J. Am. Chem. Soc.*, 2004, **126**, 11168–11169.
70 J. Lu, D. M. Ho, N. J. Vogelaar, C. M. Kraml, S. Bernhard, N. Byrne, L. R. Kim and R. A. Pascal, Synthesis, Structure, and Resolution of Exceptionally Twisted Pentacenes, *J. Am. Chem. Soc.*, 2006, **128**, 17043–17050.
71 R. S. Walters, C. M. Kraml, N. Ho, D. M. Byrne, Q. Qin, F. J. Coughlin, S. Bernhard and R. A. Pascal, Configurationally Stable Longitudinally Twisted Polycyclic Aromatic Compounds, *J. Am. Chem. Soc.*, 2008, **130**, 16435–16441.
72 J. Xiao, H. M. Duong, Y. Liu, W. Shi, L. Ji, G. Li, S. Li, X. W. Liu, J. Ma, F. Wudl and Q. Zhang, Synthesis and structure characterization of a stable nonatwistacene, *Angew Chem. Int. Ed. Engl.*, 2012, **51**, 6094–6098.
73 Y. Zhong, B. Kumar, S. Oh, M. T. Trinh, Y. Wu, K. Elbert, P. Li, X. Zhu, S. Xiao, F. Ng, M. L. Steigerwald and C. Nuckolls, Helical ribbons for molecular electronics, *J. Am. Chem. Soc.*, 2014, **136**, 8122–8130.

74 W. Fan, T. Winands, N. L. Doltsinis, Y. Li and Z. Wang, A Decatwistacene with an Overall 170 degrees Torsion, *Angew Chem. Int. Ed. Engl.*, 2017, **56**, 15373–15377.
75 W. Chen, X. Li, G. Long, Y. Li, R. Ganguly, M. Zhang, N. Aratani, H. Yamada, M. Liu and Q. Zhang, Pyrene-Containing Twistarene: Twelve Benzene Rings Fused in a Row, *Angew Chem. Int. Ed. Engl.*, 2018, **57**, 13555–13559.
76 G. Liu, C. Xiao, F. Negri, Y. Li and Z. Wang, Dodecatwistarene Imides with Zigzag-Twisted Conformation for Organic Electronics, *Angew Chem. Int. Ed. Engl.*, 2020, **59**, 2008–2012.
77 S. Castro-Fernández, C. M. Cruz, I. F. A. Mariz, I. R. Márquez, V. G. Jimenez, L. Palomino-Ruiz, J. M. Cuerva, E. Maçôas and A. G. Campaña, Two-Photon Absorption Enhancement by the Inclusion of a Tropone Ring in Distorted Nanographene Ribbons, *Angew Chem. Int. Ed. Engl.*, 2020, **59**, 7139–7145.
78 S. Ma, J. Gu, C. Lin, Z. Luo, Y. Zhu and J. Wang, Supertwistacene: A Helical Graphene Nanoribbon, *J. Am. Chem. Soc.*, 2020, **142**, 16887–16893.
79 X. Yao, W. Zheng, S. Osella, Z. Qiu, S. Fu, D. Schollmeyer, B. Muller, D. Beljonne, M. Bonn, H. I. Wang, K. Müller and A. Narita, Synthesis of Nonplanar Graphene Nanoribbon with Fjord Edges, *J. Am. Chem. Soc.*, 2021, **143**, 5654–5658.
80 P. Izquierdo-García, J. M. Fernández-García, I. Fernández, J. Perles and N. Martín, Helically Arranged Chiral Molecular Nanographenes, *J. Am. Chem. Soc.*, 2021, **143**, 11864–11870.
81 S. T. Bao, H. Jiang, C. Schaack, S. Louie, M. L. Steigerwald, C. Nuckolls and Z. Jin, Remote Control of Dynamic Twistacene Chirality, *J. Am. Chem. Soc.*, 2022, **144**, 18772–18777.
82 R. K. Dubey, M. Melle-Franco and A. Mateo-Alonso, Inducing Single-Handed Helicity in a Twisted Molecular Nanoribbon, *J. Am. Chem. Soc.*, 2022, **144**, 2765–2774.
83 Z. Sun, W. Fan, Y. Han, W. Yuan, Y. Ni, J. Wang, H. Wei, Y. Zhao, Z. Sun and J. Wu, Helical fused 1,2:8,9-dibenzozethrene oligomers with up to 201 degrees end-to-end twist: "one-pot" synthesis and chiral resolution, *Chem. Sci.*, 2023, **14**, 7922–7927.
84 W. Yang, G. Longhi, S. Abbate, A. Lucotti, M. Tommasini, C. Villani, V. J. Catalano, A. O. Lykhin, S. A. Varganov and W. A. Chalifoux, Chiral Peropyrene: Synthesis, Structure, and Properties, *J. Am. Chem. Soc.*, 2017, **139**, 13102–13109.
85 A. Link and C. Sparr, Stereoselective arene formation, *Chem. Soc. Rev.*, 2018, **47**, 3804–3815.
86 W. Liu, T. Qin, W. Xie and X. Yang, Catalytic Enantioselective Synthesis of Helicenes, *Chem.–Eur. J.*, 2022, **28**, e202202369.
87 T. Hartung, R. Machleid, M. Simon, C. Golz and M. Alcarazo, Enantioselective Synthesis of 1,12-Disubstituted [4]Helicenes, *Angew Chem. Int. Ed. Engl.*, 2020, **59**, 5660–5664.
88 F. Wang, F. Gan, C. Shen and H. Qiu, Amplifiable Symmetry Breaking in Aggregates of Vibrating Helical Molecules, *J. Am. Chem. Soc.*, 2020, **142**, 16167–16172.
89 G. Li, T. Matsuno, Y. Han, S. Wu, Y. Zou, Q. Jiang, H. Isobe and J. Wu, Fused Quinoidal Dithiophene-Based Helicenes: Synthesis by Intramolecular Radical-Radical Coupling Reactions and Dynamics of Interconversion of Enantiomers, *Angew Chem. Int. Ed. Engl.*, 2021, **60**, 10326–10333.
90 M. S. H. Salem, A. Sabri, M. I. Khalid, H. Sasai and S. Takizawa, Two-Step Synthesis, Structure, and Optical Features of a Double Hetero[7]helicene, *Molecules*, 2022, **27**, 9068.
91 T. Ikai, K. Oki, S. Yamakawa and E. Yashima, Stereospecific Synthesis of Enantiopure [6]Helicene Containing a Seven-Membered Ring and [7]Helicene by Acid-Promoted Stepwise Alkyne Annulations of Doubly Axial-Chiral Precursors, *Angew Chem. Int. Ed. Engl.*, 2023, **62**, e202301836.
92 V. M. Freixas, N. Oldani, S. Tretiak and S. Fernandez-Alberti, Twisting Aromaticity and Photoinduced Dynamics in Hexapole Helicenes, *J. Phys. Chem. Lett.*, 2023, **14**, 10145–10150.
93 S. M. Guo, S. Huh, M. Coehlo, L. Shen, G. Pieters and O. Baudoin, A C-H activation-based enantioselective synthesis of lower carbo[*n*]helicenes, *Nat. Chem.*, 2023, **15**, 872–880.
94 W. L. Xu, R. X. Zhang, H. Wang, J. Chen and L. Zhou, Helicoselective Synthesis of Indolohelicenoids through Organocatalytic Central-to-Helical Chirality Conversion, *Angew Chem. Int. Ed. Engl.*, 2024, **63**, e202318021.
95 F. Gan, G. Zhang, J. Liang, C. Shen and H. Qiu, π-Extended Diaza[7]helicenes with Dual Negatively Curved Heptagons: Extensive Synthesis and Spontaneous Resolution into Strippable Homochiral Lamellae with Helical Symmetry, *Angew Chem. Int. Ed. Engl.*, 2024, **63**, e202320076.
96 P. Jiang, A. S. Mikherdov, H. Ito and M. Jin, Crystallization-Induced Chirality Transfer in Conformationally Flexible Azahelicene Au(I) Complexes with Circularly Polarized Luminescence Activation, *J. Am. Chem. Soc.*, 2024, **146**, 12463–12472.
97 J. S. Wu, S. W. Cheng, Y. J. Cheng and C. S. Hsu, Donor-acceptor conjugated polymers based on multifused ladder-type arenes for organic solar cells, *Chem. Soc. Rev.*, 2015, **44**, 1113–1154.
98 A. Fukazawa and S. Yamaguchi, Ladder π-conjugated materials containing main-group elements, *Chem.–Asian J.*, 2009, **4**, 1386–1400.
99 J. Chen, K. Yang, X. Zhou and X. Guo, Ladder-Type Heteroarene-Based Organic Semiconductors, *Chem.–Asian J.*, 2018, **13**, 2587–2600.
100 C. Zhu, A. J. Kalin and L. Fang, Covalent and Noncovalent Approaches to Rigid Coplanar π-Conjugated Molecules and Macromolecules, *Acc. Chem. Res.*, 2019, **52**, 1089–1100.
101 Z. Xiao, S. Yang, Z. Yang, J. Yang, H. L. Yip, F. Zhang, F. He, T. Wang, J. Wang, Y. Yuan, H. Yang, M. Wang and L. Ding, Carbon-Oxygen-Bridged Ladder-Type Building Blocks for Highly Efficient Nonfullerene Acceptors, *Adv. Mater.*, 2019, **31**, e1804790.

102 S. Che and L. Fang, Porous Ladder Polymer Networks, *Chem*, 2020, **6**, 2558–2590.
103 J. Lee, Recent Progress in Synthesis of Conjugated Ladder Polymers, *Asian J. Org. Chem.*, 2023, **12**, e202300104.
104 E. M. Sánchez-Carnerero, A. R. Agarrabeitia, F. Moreno, B. L. Maroto, G. Muller, M. J. Ortiz and S. de la Moya, Circularly Polarized Luminescence from Simple Organic Molecules, *Chem.–Eur. J.*, 2015, **21**, 13488–13500.
105 Z.-L. Gong, X. Zhu, Z. Zhou, S.-W. Zhang, D. Yang, B. Zhao, Y.-P. Zhang, J. Deng, Y. Cheng, Y.-X. Zheng, S.-Q. Zang, H. Kuang, P. Duan, M. Yuan, C.-F. Chen, Y. S. Zhao, Y.-W. Zhong, B. Z. Tang and M. Liu, Frontiers in circularly polarized luminescence: molecular design, self-assembly, nanomaterials, and applications, *Sci. China: Chem.*, 2021, **64**, 2060–2104.
106 X. Yang, X. Gao, Y.-X. Zheng, H. Kuang, C.-F. Chen, M. Liu, P. Duan and Z. Tang, Recent Progress of Circularly Polarized Luminescence Materials from Chinese Perspectives, *CCS Chem.*, 2023, **5**, 2760–2789.
107 Y. Wang, Y. Yu, H. Liao, Y. Zhou, I. McCulloch and W. Yue, The Chemistry and Applications of Heteroisoindigo Units as Enabling Links for Semiconducting Materials, *Acc. Chem. Res.*, 2020, **53**, 2855–2868.
108 Y. Zhou, W. Zhang and G. Yu, Recent structural evolution of lactam- and imide-functionalized polymers applied in organic field-effect transistors and organic solar cells, *Chem. Sci.*, 2021, **12**, 6844–6878.
109 J. Cao, Q. Liao, X. Du, J. Chen, Z. Xiao, Q. Zuo and L. Ding, A pentacyclic aromatic lactam building block for efficient polymer solar cells, *Energy Environ. Sci.*, 2013, **6**, 3224–3228.
110 J. Cao, C. Zuo, B. Du, X. Qiu and L. Ding, Hexacyclic lactam building blocks for highly efficient polymer solar cells, *Chem. Commun.*, 2015, **51**, 12122–12125.
111 W. Hu, Z. Zhang, Y. Xu, J. Cao, S. Liu, Z. Tang, B. Zhao and J. Zhang, An axisymmetric heptacyclic lactam unit for efficient polymer solar cells, *J. Mater. Chem. C*, 2018, **6**, 6911–6915.
112 A. Onwubiko, W. Yue, C. Jellett, M. Xiao, H. Y. Chen, M. K. Ravva, D. A. Hanifi, A. C. Knall, B. Purushothaman, M. Nikolka, J. C. Flores, A. Salleo, J. L. Bredas, H. Sirringhaus, P. Hayoz and I. McCulloch, Fused electron deficient semiconducting polymers for air stable electron transport, *Nat. Commun.*, 2018, **9**, 416.
113 Y. Lu, Z. D. Yu, R. Z. Zhang, Z. F. Yao, H. Y. You, L. Jiang, H. I. Un, B. W. Dong, M. Xiong, J. Y. Wang and J. Pei, Rigid Coplanar Polymers for Stable n-Type Polymer Thermoelectrics, *Angew Chem. Int. Ed. Engl.*, 2019, **58**, 11390–11394.
114 N. Blouin, A. Michaud, S. Wakim, P. L. T. Boudreault, M. Leclerc, B. Vercelli, S. Zecchin and G. Zotti, Optical, Electrochemical, Magnetic, and Conductive Properties of New Polyindolocarbazoles and Polydiindolocarbazoles, *Macromol. Chem. Phys.*, 2006, **207**, 166–174.
115 T. Janosik, N. Wahlström and J. Bergman, Recent progress in the chemistry and applications of indolocarbazoles, *Tetrahedron*, 2008, **64**, 9159–9180.
116 J. Li and A. C. Grimsdale, Carbazole-based polymers for organic photovoltaic devices, *Chem. Soc. Rev.*, 2010, **39**, 2399–2410.
117 T. Janosik, A. Rannug, U. Rannug, N. Wahlström, J. Slätt and J. Bergman, Chemistry and Properties of Indolocarbazoles, *Chem. Rev.*, 2018, **118**, 9058–9128.
118 H. Jiang, S. Zhu, Z. Cui, Z. Li, Y. Liang, J. Zhu, P. Hu, H. L. Zhang and W. Hu, High-performance five-ring-fused organic semiconductors for field-effect transistors, *Chem. Soc. Rev.*, 2022, **51**, 3071–3122.
119 H. Wang, H. Zhao, S. Chen, L. Bai, Z. Su and Y. Wu, Effective Synthesis of Ladder-type Oligo(*p*-aniline)s and Poly(*p*-aniline)s via Intramolecular S_NAr Reaction, *Org. Lett.*, 2021, **23**, 2217–2221.
120 T. Ikai, T. Yoshida, K. Shinohara, T. Taniguchi, Y. Wada and T. M. Swager, Triptycene-Based Ladder Polymers with One-Handed Helical Geometry, *J. Am. Chem. Soc.*, 2019, **141**, 4696–4703.
121 W. Zheng, T. Ikai and E. Yashima, Synthesis of Single-Handed Helical Spiro-Conjugated Ladder Polymers through Quantitative and Chemoselective Cyclizations, *Angew. Chem., Int. Ed.*, 2021, **60**, 11294–11299.
122 T. Ikai, S. Miyoshi, K. Oki, R. Saha, Y. Hijikata and E. Yashima, Defect-Free Synthesis of a Fully π-Conjugated Helical Ladder Polymer and Resolution into a Pair of Enantiomeric Helical Ladders, *Angew. Chem., Int. Ed.*, 2023, **62**, e202301962.
123 T. Iwasaki, Y. Kohinata and H. Nishide, Poly(thiaheterohelicene): A Stiff Conjugated Helical Polymer Comprised of Fused Benzothiophene Rings, *Org. Lett.*, 2005, **7**, 755–758.
124 K. Takaishi, S. Hinoide, T. Matsumoto and T. Ema, Axially Chiral peri-Xanthenoxanthenes as a Circularly Polarized Luminophore, *J. Am. Chem. Soc.*, 2019, **141**, 11852–11857.
125 T. Ikai, N. Mishima, T. Matsumoto, S. Miyoshi, K. Oki and E. Yashima, 2,2'-Tethered Binaphthyl-Embedded One-Handed Helical Ladder Polymers: Impact of the Tether Length on Helical Geometry and Chiroptical Property, *Angew. Chem., Int. Ed.*, 2024, **63**, e202318712.
126 H.-C. Zhang and L. Pu, Synthesis of Helical Polybinaphthyls, *Macromolecules*, 2004, **37**, 2695–2702.
127 R. Ammenhäuser, J. M. Lupton and U. Scherf, Chain-Length Dependence of the Optical Activity of Helical Triptycene-Based π-Conjugated Ladder Polymers, *Adv. Opt. Mater.*, 2024, **12**, 2301857.
128 R. Fiesel, J. Huber and U. Scherf, Synthesis of an Optically Active Poly(*para*-phenylene) Ladder Polymer, *Angew. Chem., Int. Ed.*, 1996, **35**, 2111–2113.
129 W. Zheng, K. Oki, R. Saha, Y. Hijikata, E. Yashima and T. Ikai, One-Handed Helical Tubular Ladder Polymers for Chromatographic Enantioseparation, *Angew. Chem., Int. Ed.*, 2023, **62**, e202218297.
130 R. Ammenhäuser, P. Klein, E. Schmid, S. Streicher, J. Vogelsang, C. W. Lehmann, J. M. Lupton, S. C. J. Meskers and U. Scherf, Circularly Polarized Light Probes Excited-State Delocalization in Rectangular

Ladder-type Pentaphenyl Helices, *Angew. Chem., Int. Ed.*, 2023, **62**, e202211946.

131 X. Xiao, Q. Cheng, S. Bao, Z. Jin, S. Sun, H. Jiang, M. L. Steigerwald and C. Nuckolls, Single-Handed Helicene Nanoribbons via Transfer of Chiral Information, *J. Am. Chem. Soc.*, 2022, **144**, 20214–20220.

132 A. C. Grimsdale and K. Müllen, Oligomers and Polymers Based on Bridged Phenylenes as Electronic Materials, *Macromol. Rapid Commun.*, 2007, **28**, 1676–1702.

133 J. Lee, B. B. Rajeeva, T. Yuan, Z. H. Guo, Y. H. Lin, M. Al-Hashimi, Y. Zheng and L. Fang, Thermodynamic synthesis of solution processable ladder polymers, *Chem. Sci.*, 2016, **7**, 881–889.

134 J. Lee, A. J. Kalin, T. Yuan, M. Al-Hashimi and L. Fang, Fully conjugated ladder polymers, *Chem. Sci.*, 2017, **8**, 2503–2521.

135 L. Fang, A. Kalin and J. Lee, Annulation Reactions for Conjugated Ladder-Type Oligomers, *Synlett*, 2018, **29**, 993–998.

136 Z. D. Yu, Y. Lu, J. Y. Wang and J. Pei, Conformation Control of Conjugated Polymers, *Chem.–Eur. J.*, 2020, **26**, 16194–16205.

137 Y. Dong, J. Ma, S. Yang and H. Yang, Polyimides and Their Diverse Applications in Multiple Optoelectronic Devices, *Adv. Devices Instrum.*, 2023, **4**, 0011.

138 H. Fan, H. Zhao and Y. Wu, Progress in conjugated ladder polymers, *Sci. Sin.: Chim.*, 2021, **51**, 1150–1167.

139 J. J. Stewart, Optimization of parameters for semiempirical methods VI: more modifications to the NDDO approximations and re-optimization of parameters, *J. Mol. Model.*, 2013, **19**, 1–32.

140 D. Alberico, M. E. Scott and M. Lautens, Aryl–Aryl Bond Formation by Transition-Metal-Catalyzed Direct Arylation, *Chem. Rev.*, 2007, **107**, 174–238.

141 W. Hagui, H. Doucet and J.-F. Soulé, Application of Palladium-Catalyzed C(sp2)–H Bond Arylation to the Synthesis of Polycyclic (Hetero)Aromatics, *Chem*, 2019, **5**, 2006–2078.

142 L.-C. Campeau, M. Parisien, M. Leblanc and K. Fagnou, Biaryl Synthesis via Direct Arylation: Establishment of an Efficient Catalyst for Intramolecular Processes, *J. Am. Chem. Soc.*, 2004, **126**, 9186–9187.

143 D. García-Cuadrado, A. A. C. Braga, F. Maseras and A. M. Echavarren, Proton Abstraction Mechanism for the Palladium-Catalyzed Intramolecular Arylation, *J. Am. Chem. Soc.*, 2006, **128**, 1066–1067.

144 K. E. Yamada, I. A. Stepek, W. Matsuoka, H. Ito and K. Itami, Synthesis of Heptagon-Containing Polyarenes by Catalytic C-H Activation, *Angew Chem. Int. Ed. Engl.*, 2023, **62**, e202311770.

145 H. Xie, Z. Xiao, Y. Song, K. Jin, H. Liu, E. Zhou, J. Cao, J. Chen, J. Ding, C. Yi, X. Shen, C. Zuo and L. Ding, Tethered Helical Ladder-Type Aromatic Lactams, *J. Am. Chem. Soc.*, 2024, **146**, 11978–11990.

146 K. Takagi, D. Miyamoto, H. Yamaguchi and I. Azumaya, Toward the Synthesis of a Belt-Shaped Cyclic π-Conjugated System Comprising para-Phenylene Framework and Amide Bridging Unit, *Bull. Chem. Soc. Jpn.*, 2022, **95**, 47–51.

147 F. P. Gasparro and N. H. Kolodny, NMR determination of the rotational barrier in N,N-dimethylacetamide. A physical chemistry experiment, *J. Chem. Educ.*, 1977, **54**, 258–261.

148 V. Štejfa, S. Chun, V. Pokorný, M. Fulem and K. Růžička, Thermodynamic study of acetamides, *J. Mol. Liq.*, 2020, **319**, 114019.

149 P. Kiraly, G. Dal Poggetto, L. Castanar, M. Nilsson, A. Deák and G. A. Morris, Broadband measurement of true transverse relaxation rates in systems with coupled protons: application to the study of conformational exchange, *Chem. Sci.*, 2021, **12**, 11538–11547.

150 N. G. Malliaros and M. Orfanopoulos, One-step photocatalyzed functionalization of [60]Fullerene: A study on the direct incorporation of amides and lactams to C60, *J. Phys. Chem. Solids*, 2023, **178**, 111305.

151 Z. Chen, C. S. Wannere, C. Corminboeuf, R. Puchta and P. v. R. Schleyer, Nucleus-Independent Chemical Shifts (NICS) as an Aromaticity Criterion, *Chem. Rev.*, 2005, **105**, 3842–3888.

152 P. v. R. Schleyer, C. Maerker, A. Dransfeld, H. Jiao and N. J. R. van Eikema Hommes, Nucleus-Independent Chemical Shifts: A Simple and Efficient Aromaticity Probe, *J. Am. Chem. Soc.*, 1996, **118**, 6317–6318.

153 M. Krzeszewski, H. Ito and K. Itami, Infinitene: A Helically Twisted Figure-Eight [12]Circulene Topoisomer, *J. Am. Chem. Soc.*, 2022, **144**, 862–871.

154 M. Toya, T. Omine, F. Ishiwari, A. Saeki, H. Ito and K. Itami, Expanded [2,1][*n*]Carbohelicenes with 15- and 17-Benzene Rings, *J. Am. Chem. Soc.*, 2023, **145**, 11553–11565.

155 S. E. Wheeler, K. N. Houk, P. V. R. Schleyer and W. D. Allen, A hierarchy of homodesmotic reactions for thermochemistry, *J. Am. Chem. Soc.*, 2009, **131**, 2547–2560.

156 M. Tang, Y. Liang, X. Lu, X. Miao, L. Jiang, J. Liu, L. Bian, S. Wang, L. Wu and Z. Liu, Molecular-strain engineering of double-walled tetrahedra, *Chem*, 2021, **7**, 2160–2174.

157 P. K. Saha, A. Mallick, A. T. Turley, A. N. Bismillah, A. Danos, A. P. Monkman, A.-J. Avestro, D. S. Yufit and P. R. McGonigal, Rupturing aromaticity by periphery overcrowding, *Nat. Chem.*, 2023, **15**, 516–525.

158 Y. Tanaka, K. Tajima, R. Kusumoto, Y. Kobori, N. Fukui and H. Shinokubo, End-to-End Bent Perylene Bisimide Cyclophanes by Double Sulfur Extrusion, *J. Am. Chem. Soc.*, 2024, **146**, 16332–16339.

159 M. M. Safont-Sempere, P. Osswald, M. Stolte, M. Grune, M. Renz, M. Kaupp, K. Radacki, H. Braunschweig and F. Würthner, Impact of molecular flexibility on binding strength and self-sorting of chiral π-surfaces, *J. Am. Chem. Soc.*, 2011, **133**, 9580–9591.

160 B. Mahlmeister, T. Schembri, V. Stepanenko, K. Shoyama, M. Stolte and F. Würthner, Enantiopure J-Aggregate of Quaterrylene Bisimides for Strong Chiroptical NIR-Response, *J. Am. Chem. Soc.*, 2023, **145**, 13302–13311.

161 X. Yang, M. Brückner, F. Rominger, T. Kirschbaum and M. Mastalerz, Dispersion-driven formation of chiral twisted PAH double helices, *Chem*, 2024, **10**, 832–842.
162 T. Lu and Q. Chen, Independent gradient model based on Hirshfeld partition: A new method for visual study of interactions in chemical systems, *J. Comput. Chem.*, 2022, **43**, 539–555.
163 C. Lefebvre, G. Rubez, H. Khartabil, J. C. Boisson, J. Contreras-García and E. Henon, Accurately extracting the signature of intermolecular interactions present in the NCI plot of the reduced density gradient versus electron density, *Phys. Chem. Chem. Phys.*, 2017, **19**, 17928–17936.
164 T. Lu and F. Chen, Multiwfn: a multifunctional wavefunction analyzer, *J. Comput. Chem.*, 2012, **33**, 580–592.
165 W. Humphrey, A. Dalke and K. Schulten, VMD: Visual molecular dynamics, *J. Mol. Graphics Modell.*, 1996, **14**, 33–38.
166 T. Lu and Q. Chen, Interaction Region Indicator: A Simple Real Space Function Clearly Revealing Both Chemical Bonds and Weak Interactions, *Chem.: Methods*, 2021, **1**, 231–239.
167 F. Neese, Software update: The ORCA program system—Version 5.0, *Wiley Interdiscip. Rev.: Comput. Mol. Sci.*, 2022, **12**, e1606.
168 S. Grimme, A. Hansen, S. Ehlert and J. M. Mewes, r(2)SCAN-3c: A "Swiss army knife" composite electronic-structure method, *J. Chem. Phys.*, 2021, **154**, 064103.
169 T. Gasevic, J. B. Stuckrath, S. Grimme and M. Bursch, Optimization of the r(2)SCAN-3c Composite Electronic-Structure Method for Use with Slater-Type Orbital Basis Sets, *J. Phys. Chem. A*, 2022, **126**, 3826–3838.
170 J. B. Birks, Excimers, *Rep. Prog. Phys.*, 1975, **38**, 903–974.
171 H. Saigusa and E. C. Lim, Excimer Formation in van der Waals Dimers and Clusters of Aromatic Molecules, *Acc. Chem. Res.*, 1996, **29**, 171–178.
172 F. M. Winnik, Photophysics of preassociated pyrenes in aqueous polymer solutions and in other organized media, *Chem. Rev.*, 1993, **93**, 587–614.
173 H. Liu, L. Shen, Z. Cao and X. Li, Covalently linked perylenetetracarboxylic diimide dimers and trimers with rigid "*J*-type" aggregation structure, *Phys. Chem. Chem. Phys.*, 2014, **16**, 16399–16406.
174 J. M. Robertson and J. G. White, 72, The crystal structure of pyrene. A quantitative X-ray investigation, *J. Chem. Soc.*, 1947, 358–368.
175 J. Ferguson, Absorption and Fluorescence Spectra of Crystalline Pyrene, *J. Chem. Phys.*, 1958, **28**, 765–768.
176 J. B. Birks, A. A. Kazzaz and T. A. King, Excimer' Fluorescence - IX. Lifetime Studies of Pyrene Crystals, *Proc. R. Soc. London, Ser. A*, 1997, **291**, 556–569.
177 F. Würthner, Z. Chen, V. Dehm and V. Stepanenko, One-dimensional luminescent nanoaggregates of perylene bisimides, *Chem. Commun.*, 2006, 1188–1190, DOI: 10.1039/b517020f.
178 Z. Chen, U. Baumeister, C. Tschierske and F. Würthner, Effect of core twisting on self-assembly and optical properties of perylene bisimide dyes in solution and columnar liquid crystalline phases, *Chem.–Eur. J.*, 2007, **13**, 450–465.
179 L. Arrico, L. Di Bari and F. Zinna, Quantifying the Overall Efficiency of Circularly Polarized Emitters, *Chem.–Eur. J.*, 2021, **27**, 2920–2934.
180 H. Tanaka, Y. Inoue and T. Mori, Circularly Polarized Luminescence and Circular Dichroisms in Small Organic Molecules: Correlation between Excitation and Emission Dissymmetry Factors, *ChemPhotoChem*, 2018, **2**, 386–402.
181 Y. Zhang, S. Yu, B. Han, Y. Zhou, X. Zhang, X. Gao and Z. Tang, Circularly polarized luminescence in chiral materials, *Matter*, 2022, **5**, 837–875.
182 Z. L. Gong, Z. Q. Li and Y. W. Zhong, Circularly polarized luminescence of coordination aggregates, *Aggregate*, 2022, **3**, e177.
183 T. Zhang, Y. Zhang, Z. He, T. Yang, X. Hu, T. Zhu, Y. Zhang, Y. Tang and J. Jiao, Recent Advances of Chiral Isolated and Small Organic Molecules: Structure and Properties for Circularly Polarized Luminescence, *Chem.–Asian J.*, 2024, **19**, e202400049.
184 K. Takaishi, S. Murakami, F. Yoshinami and T. Ema, Binaphthyl-Bridged Pyrenophanes: Intense Circularly Polarized Luminescence Based on a D_2 Symmetry Strategy, *Angew Chem. Int. Ed. Engl.*, 2022, **61**, e202204609.
185 J. Wang, G. Zhuang, M. Chen, D. Lu, Z. Li, Q. Huang, H. Jia, S. Cui, X. Shao, S. Yang and P. Du, Selective Synthesis of Conjugated Chiral Macrocycles: Sidewall Segments of (-)/(+)-(12,4) Carbon Nanotubes with Strong Circularly Polarized Luminescence, *Angew Chem. Int. Ed. Engl.*, 2020, **59**, 1619–1626.
186 W. L. Zhao, M. Li, H. Y. Lu and C. F. Chen, Advances in helicene derivatives with circularly polarized luminescence, *Chem. Commun.*, 2019, **55**, 13793–13803.
187 J. L. Ma, Q. Peng and C. H. Zhao, Circularly Polarized Luminescence Switching in Small Organic Molecules, *Chem.–Eur. J.*, 2019, **25**, 15441–15454.
188 Y. Liu, Z. Ma, Z. Wang and W. Jiang, Boosting Circularly Polarized Luminescence Performance by a Double π-Helix and Heteroannulation, *J. Am. Chem. Soc.*, 2022, **144**, 11397–11404.
189 Z. Wei, Y. Yang and L. Liu, Chiral Organic Optoelectronic Materials and Circularly Polarized Light Luminescence and Detection, *Acta Chim. Sin.*, 2022, **80**, 970–992.
190 M. Hasegawa, C. Hasegawa, Y. Nagaya, K. Tsubaki and Y. Mazaki, Multiply Twisted Chiral Macrocycles Clamped by Tethered Binaphthyls Exhibiting High Circularly Polarized Luminescence Brightness, *Chem.–Eur. J.*, 2022, **28**, e202202218.
191 A. Morisaki, R. Inoue and Y. Morisaki, Synthesis of Two Novel Optically Active #-Shaped Cyclic Tetramers Based on Planar Chiral [2.2]Paracyclophanes, *Chem.–Eur. J.*, 2023, **29**, e202203533.

192 Y. J. Shen, N. T. Yao, L. N. Diao, Y. Yang, X. L. Chen and H. Y. Gong, A -Extended Pentadecabenzo[9]Helicene, *Angew Chem. Int. Ed. Engl.*, 2023, **62**, e202300840.

193 W. Niu, Y. Fu, Z. L. Qiu, C. J. Schurmann, S. Obermann, F. Liu, A. A. Popov, H. Komber, J. Ma and X. Feng, π-Extended Helical Multilayer Nanographenes with Layer-Dependent Chiroptical Properties, *J. Am. Chem. Soc.*, 2023, **145**, 26824–26832.

194 Y. Liu, Z. Li, M. W. Wang, J. Chan, G. Liu, Z. Wang and W. Jiang, Highly Luminescent Chiral Double π-Helical Nanoribbons, *J. Am. Chem. Soc.*, 2024, **146**, 5295–5304.

195 A. Bedi and O. Gidron, The Consequences of Twisting Nanocarbons: Lessons from Tethered Twisted Acenes, *Acc. Chem. Res.*, 2019, **52**, 2482–2490.

196 Y. Liang, M. Tang and Z. Liu, Molecular Bows—Strained Bow-shaped Macrocycles, *Chem. Lett.*, 2020, **49**, 1329–1336.

197 J. Liu, M. Wu, L. Wu, Y. Liang, Z. B. Tang, L. Jiang, L. Bian, K. Liang, X. Zheng and Z. Liu, Infinite Twisted Polycatenanes, *Angew. Chem., Int. Ed.*, 2023, **62**, e202314481.

198 L. Jiang, Z. Peng, Y. Liang, Z. B. Tang, K. Liang, J. Liu and Z. Liu, Strain-Driven Formal [1,3]-Aryl Shift within Molecular Bows, *Angew. Chem., Int. Ed.*, 2023, **62**, e202314481.

199 M. Tang, Y. Liang, J. Liu, L. Bian and Z. Liu, Mechanical Trapping of the Phlorin Intermediate, *CCS Chem.*, 2022, **4**, 3230–3237.

200 M. Tang, Y. Liang, J. Liu, L. Wu, S. Wang, L. Bian, L. Jiang, Z. B. Tang and Z. Liu, Mechanical trapping and in situ derivatization of the porphodimethene intermediate, *Mater. Today Chem.*, 2022, **24**, 100868.

201 L. Wu, M. Tang, L. Jiang, Y. Chen, L. Bian, J. Liu, S. Wang, Y. Liang and Z. Liu, Synthesis of contra-helical trefoil knots with mechanically tuneable spin-crossover properties, *Nat. Synth.*, 2022, **2**, 17–25.

202 K. Liang, Y. Liang, M. Tang, J. Liu, Z.-B. Tang and Z. Liu, π-Diamond: A Diamondoid Superstructure Driven by π-Interactions, *Angew. Chem., Int. Ed.*, 2024, **63**, e202409507.

203 P. Osswald, M. Reichert, G. Bringmann and F. Würthner, Perylene Bisimide Atropisomers: Synthesis, Resolution, and Stereochemical Assignment, *J. Org. Chem.*, 2007, **72**, 3403–3411.

204 B. Sadowski, D. Mierzwa, S. Kang, M. Grzybowski, Y. M. Poronik, A. L. Sobolewski, D. Kim and D. T. Gryko, Tuning the aromatic backbone twist in dipyrrolonaphthyridinediones, *Chem. Commun.*, 2022, **58**, 3697–3700.

205 A. Bedi and O. Gidron, Chiroptical Properties of Twisted Acenes: Experimental and Computational Study, *Chem.–Eur. J.*, 2019, **25**, 3279–3285.

206 A. Bedi, L. J. W. Shimon and O. Gidron, Helically Locked Tethered Twistacenes, *J. Am. Chem. Soc.*, 2018, **140**, 8086–8090.

207 A. Bedi, G. Schwartz, U. Hananel, A. Manor Armon, I. Shioukhi, G. Markovich and O. Gidron, The effect of axial and helical chirality on circularly polarized luminescence: lessons learned from tethered twistacenes, *Chem. Commun.*, 2023, **59**, 2011–2014.